JOURNAL OF GEOPHYSICAL RESEARCH, VOL. 114, B00A06, doi:10.1029/2008JB006049, 2009

Remote triggering of tremor along the San Andreas Fault in central California

Zhigang Peng,[1] John E. Vidale,[2] Aaron G. Wech,[2] Robert M. Nadeau,[3] and Kenneth C. Creager[2]

Received 30 August 2008; accepted 16 April 2009; published 18 July 2009.

[1] We perform a systematic survey of triggered tremor along the San Andreas Fault in central California for the 31 teleseismic earthquakes with Mw $\geq$ 7.5 since 2001. We identify 10 teleseismic events associated with clear triggered tremor. About 52% of the tremor is concentrated south of Parkfield near Cholame, where ambient tremor has been identified previously, and the rest is widely distributed in the creeping section of the San Andreas Fault north of Parkfield. Tremor is generally initiated and is in phase with the Love wave particle velocity. However, the pattern becomes complicated with the arrival of the Rayleigh waves, and sometimes tremor continues after the passage of the surface waves. We identify two cases in which tremor is triggered during the teleseismic *PKP* phase. These results suggest that while shear stress from the passage of the Love waves plays the most important role in triggering tremor in central California, other factors, such as dilatational stresses from the Rayleigh and *P* waves, also contribute. We also examine the ambient tremor occurrence rate before and after the teleseismic events and find a transient increase of stacked tremor rate during the passage of the teleseismic surface waves. This observation implies that the occurrence time of tremor is temporally advanced by the dynamic stresses of the teleseismic waves. The amplitude of the teleseismic waves correlates with the occurrence of triggered tremor, and the inferred tremor-triggering threshold is $\sim$2–3 kPa. The relatively low triggering threshold indicates that the effective stress at the tremor source region is very low, most likely due to near-lithostatic fluid pressure.

Citation: Peng, Z., J. E. Vidale, A. G. Wech, R. M. Nadeau, and K. C. Creager (2009), Remote triggering of tremor along the San Andreas Fault in central California, *J. Geophys. Res.*, *114*, B00A06, doi:10.1029/2008JB006049.

1. Introduction

[2] Active plate boundary faults accommodate the majority of the deformation from far-field plate motion. The accumulated stress on these faults is mainly released by sudden brittle failure that generates earthquakes in the seismogenic zone and by continuous slow slip at shallower and deeper depth. In the region between these differing modes of relaxation, faults can release stress through transient slow slip events with durations ranging from days to years [e.g., *Dragert et al.*, 2001; *Hirose et al.*, 1999; *Lowry et al.*, 2001; *Miller et al.*, 2002]. While some slow slip events generate no observable seismic signals (so-called silent earthquakes), recent studies have identified tremor-like seismic events during episodes of slow slip events in Cascadia [*Brudzinski and Allen*, 2007; *Rogers and Dragert*, 2003] and southwest Japan [*Hirose and Obara*, 2005; *Obara and Hirose*, 2006; *Obara et al.*, 2004]. *Rogers and Dragert* [2003] termed the coupled phenomenon as episodic tremor and slip (ETS). Compared to regular earthquakes, the noise-like tremor signals have long durations and no clear impulsive phases but are coherent among stations that are several tens of kilometers apart. The tremor observed in these studies occurs in a nonvolcanic setting but has similar character to seismic tremor typically observed around volcanoes. While some tremor at volcanoes may be related directly to magma movement [e.g., *Chouet*, 1996], some may differ from what is recently observed only in the source of the causative stresses but not in the underlying generative mechanisms. Hence, in this study we use the general term "tremor" to refer to such seismic signals, rather than the term "nonvolcanic tremor" that has been widely used before.

[3] Tremor was first identified over a broad region in the subduction zone southwest of Japan [*Obara*, 2002], and was subsequently found at many places in the circum-Pacific subduction zones [e.g., *Brudzinski and Allen*, 2007; *Brudzinski*, 2008; *Payero et al.*, 2008; *Rogers and Dragert*, 2003; *Rubinstein et al.*, 2009b; *Schwartz and Rokosky*, 2007]. Recent studies have found that in addition to occurring during protracted ETS episodes, tremor can be

[1]School of Earth and Atmospheric Sciences, Georgia Institute of Technology, Atlanta, Georgia, USA.
[2]Department of Earth and Space Sciences, University of Washington, Seattle, Washington, USA.
[3]Berkeley Seismological Laboratory, University of California, Berkeley, California, USA.

0148-0227/09/2008JB006049$09.00

instantaneously triggered during the surface waves of teleseismic events in subduction zone environments [*Miyazawa and Brodsky*, 2008; *Miyazawa and Mori*, 2005, 2006; *Miyazawa et al.*, 2008; *Rubinstein et al.*, 2007, 2009a]. Furthermore, ambient (i.e., not triggered by the teleseismic waves) and triggered tremor has been observed in transform fault environments in California [*Gomberg et al.*, 2008a; *Nadeau and Dolenc*, 2005; *Peng et al.*, 2008; *Shelly et al.*, 2009; *Nadeau and Guilhem*, 2009; A. Ghosh et al., Complex nonvolcanic tremor near Parkfield triggered by the great Mw 9.2 Sumatra earthquake, submitted to *Journal of Geophysical Research*, 2009] and Japan [*Ohmi et al.*, 2004], and beneath the central Range in Taiwan, an arc-continental-type collision environment [*Peng and Chao*, 2008], indicating that the conditions for tremor generation are not confined to the subduction zone environment.

[4] Despite these new observations, the underlying mechanisms of tremor generation remain mysterious. Although several studies have suggested that the necessary conditions existed in a wide range of tectonic environments [e.g., *Gomberg et al.*, 2008a], it is still not clear what is the most important one that controls tremor generation. On the basis of the wide distribution of tremor depth, earlier studies have proposed that tremor is generated by fluid migration due to dehydration from the subducted slab [*Kao et al.*, 2005; *Obara*, 2002]. However, other recent studies have suggested that much of tremor activity is a superposition of many simple shear failure events (i.e., low-frequency earthquakes) on the plate interface [*Houston and Vidale*, 2007; *Ide et al.*, 2007a, 2007b; *Shelly et al.*, 2007a, 2007b, 2009]. This interpretation is also supported by the accurate locations of tremor and low-frequency earthquakes near the plate interface [*La Rocca et al.*, 2009; *Shelly et al.*, 2006].

[5] In regards to triggered tremor, it has been proposed that triggered tremors are set off by fluid flow due to changes in dilatational stresses associated with the Rayleigh waves [*Miyazawa and Brodsky*, 2008; *Miyazawa and Mori*, 2005, 2006; *Miyazawa et al.*, 2008], while others suggested that tremors are instantaneously triggered by changes of Coulomb failure stresses on the fault interface [*Peng and Chao*, 2008; *Peng et al.*, 2008; *Rubinstein et al.*, 2007, 2009a; Ghosh et al., submitted manuscript, 2009]. In addition, many studies have found that the dynamic stresses associated with the teleseismically triggered tremor are on the order of a few tens of kilopascals or less [*Miyazawa and Brodsky*, 2008; *Peng and Chao*, 2008; *Peng et al.*, 2008; *Rubinstein et al.*, 2007, 2009a; Ghosh et al., submitted manuscript, 2009]. However, it is still not clear whether there is a common triggering threshold for tremor generation and how it varies with amplitude and frequency. A systematic survey of tremor triggered by many teleseismic events would allow us to distinguish among different triggering mechanisms, and identify potential triggering thresholds and controlling factors for the occurrence of triggered tremor. A better understanding of where, when, and how tremor is triggered would also provide fundamental insights into the underlying mechanisms of tremor generation and the nature of fault mechanics.

[6] In this study, we conduct a systematic survey of tremor triggered by teleseismic events along the San Andreas Fault (SAF) in central California. We focus on triggered tremor in central California instead of ambient tremor or ETS at other regions for the following reasons:

[7] 1. Triggered tremor often has larger amplitude than ambient tremor or ETS events [*Peng et al.*, 2008; *Rubinstein et al.*, 2007], and is modulated by the surface waves of the teleseismic events. The relatively high signal-to-noise ratio (SNR), regular patterns, and short time window allow identification of triggered tremor in a focused region more efficiently than scanning through years of continuous data, as required for ambient tremor identification.

[8] 2. The transient stress evolution during surface waves that trigger tremor can be estimated from the nearby broadband recordings, allowing us to calibrate stimulus and response and thus discriminate between triggering mechanisms.

[9] 3. The SAF in central California and its surrounding regions had dense permanent seismic networks for several decades, providing an extensive data set for identifying triggered tremor.

[10] 4. Ambient and triggered tremor is already known to strike this region [e.g., *Gomberg et al.*, 2008a; *Nadeau and Dolenc*, 2005; *Peng et al.*, 2008; *Shelly et al.*, 2009]. The existence of a complete tremor catalog [*Nadeau and Guilhem*, 2009] allow us to place the newly identified triggered tremor in the context of regularly occurred ambient tremor and study possible changes in tremor activity before, during, and after the passage of the teleseismic waves.

[11] The organization of this article is as follows. We first describe the tectonic settings and briefly review previous studies of tremor along the SAF in central California. Then we outline the analysis procedure in section 3 and summarize the locations of tremor in section 4. In section 5, we examine each of the 10 teleseismic events that have triggered tremor in detail, and summarize the relationship between tremor occurrence and telseismic surface waves. In section 6, we quantify the triggering threshold both in amplitude and frequency. Finally, we document changes of ambient tremor occurrence during and after the surface waves of teleseismic events.

2. Tectonic Setting and Previous Studies of Tremor in Central California

[12] The SAF in central California expresses itself as a relatively straight fault on the surface. However, its frictional behavior is rather complex at depth. The Parkfield section of the SAF (Figure 1) straddles the transition between the creeping segment of the fault to the northwest and the locked segment to the southeast that last broke in the great 1857 Mw7.8 Fort Tejon earthquake [*Sieh*, 1978]. At least seven characteristic earthquakes of ~M6 occurred near Parkfield since 1857, with the most recent on 28 September 2004 [*Bakun et al.*, 2005]. The quasiperiodicity of the previous 6 events led to the deployment of many seismic and geodetic instruments as part of the Parkfield Earthquake Prediction Experiment [*Bakun and Lindh*, 1985]. The instrumentation was further augmented with the recent development of the San Andreas Fault Observatory at Depth (SAFOD) project [*Hickman et al.*, 2004].

[13] On the basis of the analysis of continuous recordings from the borehole High-Resolution Seismic Network

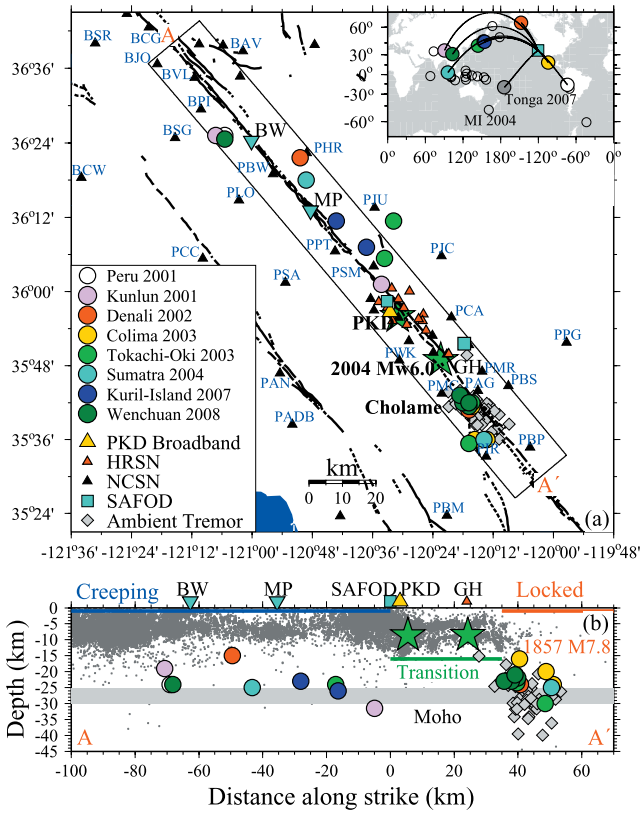

Figure 1. (a) A map of the study area along the San Andreas Fault (SAF) in central California. The dark lines denote surface traces of faults. Seismic stations of the HRSN and NCSN are denoted with red and black triangles, respectively. The broadband station PKD is shown as a yellow triangle. The hypocenters of the 1966 and 2004 Mw6.0 Parkfield earthquakes are marked with green stars. The ambient tremor previously identified [*Nadeau and Dolenc*, 2005] is denoted as the gray diamonds. The source regions for the triggered tremor are denoted as circles with different colors corresponding to different teleseismic events. Select station names are marked. The inverted triangles mark the locations of Bitterwater (BW) and Monarch Peak (MP) in the creeping section of the SAF. GH stands for Gold Hill. The inset shows the locations of the 31 teleseismic events and the great circle path of the 10 events that have triggered tremor around Parkfield. MI 2004, the Mw8.1 13 December 2004 Macquarie Islands earthquake. (b) Cross section of seismicity and location of tremor sources along AA′ in Figure 1a. The gray dots denote earthquakes since 1984 listed in the NCSN catalog. The Moho depth of 25–30 km in this region [*McBride and Brown*, 1986] is marked as a gray band. The blue, green, and red lines mark the approximate creeping, transition, and locked segments on the SAF.

(HRSN) and surface stations in the Southern California Seismic Network (SCSN), *Nadeau and Dolenc* [2005] found clear evidence of tremor around the SAF near Cholame south of Parkfield, the inferred epicentral region of the 1857 Mw7.8 Fort Tejon earthquake [*Sieh*, 1978]. The tremor found near Cholame appears to be very similar in characteristics (e.g., depth, frequency content, polarization direction, predominance of shear waves) to that found around the circum-Pacific subduction zones [e.g., *Obara*, 2002; *Rogers and Dragert*, 2003; *Schwartz and Rokosky*, 2007], except that the SAF tremor is less frequent, with shorter duration and smaller amplitude [*Nadeau and Dolenc*, 2005; *Ellsworth*, 2008]. In addition, precise locations of tremor near Cholame by *Shelly et al.* [2009] have shown near-linear structures parallel to the SAF strike, suggesting that at least a portion of the tremor occurs on the deep extension of the fault and likely represents shear slip, similar to those found at other subduction zones [e.g., *Shelly et al.*, 2007a, 2007b].

[14] Recently, *Gomberg et al.* [2008a] found tremor triggered by the 2002 Mw7.8 Denali Fault earthquake at seven locations along the entire SAF system in California, with two of them in central California. *Peng et al.* [2008] analyzed theses two tremor sources triggered by the Denali Fault earthquake in detail, and found that they originate near the base of seismogenic zone along the SAF, and are excited when the Love waves impart right-lateral shear stress and encourage slip on the SAF. Ghosh et al. (submitted manuscript, 2009) found similar results for the tremor triggered by the 2004 Mw9.2 Sumatra earthquake. In addition, they identified tremor associated with the passage of teleseismic *P* waves, suggesting that dilatational stress may also be important in triggering tremor.

3. Analysis Procedure

[15] In this study, we focus on tremor triggered by large teleseismic earthquakes along the SAF in central California. We use primarily waveforms recorded by the broadband station PKD of the Berkeley Digital Seismic Network (BDSN), surface short-period stations of the Northern California Seismic Network (NCSN), and 13 borehole short-period stations of the HRSN. We select the 31 teleseismic earthquakes listed in the ANSS catalog that occurred since 1 May 2001 (the starting time of the continuous HRSN recordings) with moment magnitude Mw $\geq$ 7.5, hypocentral depth < 100 km, and great circle distance to station PKD Δ_{PKD} > 1000 km (Table S1 in the auxiliary material).[1] We focus only on large and shallow events because those events are most effective in generating large surface waves at teleseismic distances, and hence have the greatest potential of triggering earthquakes and tremor. These 31 teleseismic events generate peak ground velocity (PGV) in the transverse component ranging from 0.0013 to 0.388 cm s^{-1} recorded at station PKD (Figure 2). Next, we download continuous waveforms for the 5 h before and after the origin time of the teleseismic event, recorded by station PKD (40 or 80 samples s^{-1}) and the HRSN (20 samples s^{-1}) from the Northern California Earthquake Data Center (NCEDC). To augment tremor identification and location, we also download the continuous high-sampling data recorded by the NCSN for selected events that are archived at the NCEDC.

[16] We identify triggered tremor as bursts of high-frequency (~2–8 Hz), nonimpulsive seismic energy that are coherent among many stations and during the passage of

[1] Auxiliary materials are available in the HTML. doi:10.1029/2008JB006049.

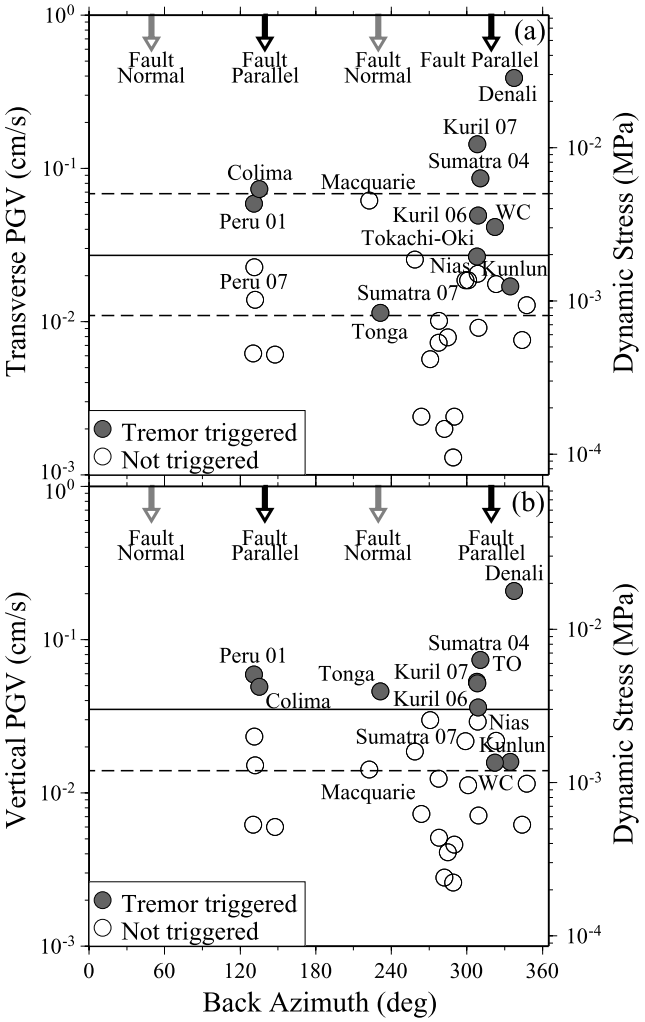

Figure 2. Peak ground velocities (left vertical axis) and the corresponding dynamic stresses (right vertical axis) for the (a) transverse and (b) vertical components measured at the broadband station PKD plotted against the back azimuth for the 31 earthquakes with Mw $\geq$ 7.5 since 2001. The 10 events that triggered clear tremors are marked with gray circles, and the rest are marked with open circles. The earthquake source information is listed in Table S1. The solid and gray arrows mark the directions parallel and perpendicular to the SAF strike (139.2° from the north). The solid line in Figure 2a marks the stress level of 2 kPa. The bottom dashed line marks the stress level of 0.8 kPa below which no earthquakes trigger tremor, and the top dashed line marks the stress level of 5 kPa above which all earthquakes trigger tremor. The solid line in Figure 2b marks the stress level of 3 kPa. The dashed line marks the stress level of 1.2 kPa below which no earthquakes trigger tremor. WC, 2008 Mw7.9 Wenchuan earthquake; TO, 2003 Mw8.3 Tokachi-Oki earthquake.

teleseismic body and surface waves (e.g., Figure 3). To rule out the possibility of instrumental artifacts at each station [*Hellweg et al.*, 2008], we require that the tremor-like signals be recorded by at least 5 stations that are separated by at least 10 km. Next, we visually scan through all the records and find a total of 10 events that triggered clear tremor in central California, including the 2 November 2002 Mw7.9 Denali Fault earthquake [*Gomberg et al.*, 2008a; *Peng et al.*, 2008], and the 26 December 2004 Mw9.2 Sumatra earthquake (Ghosh et al., submitted manuscript, 2009) that have been analyzed previously. The related parameters for these events are listed in Table S1.

[17] We locate the triggered tremor by cross-correlating all station pairs with clear tremor signals and performing a 3-D grid search that predicts the best matching *S* wave arrival times [*Wech and Creager*, 2008]. In detail, we apply a band-pass filter of 2–6 Hz, take the envelope function, low-pass filter the envelope at 0.1 Hz, and then decimate to 1 sample per second. Next, we calculate the cross correlograms for each pair of envelope functions. For each trial source location we calculate the *S* wave travel time difference to each station pair and determine the value of the correlation at the predicted lag time. We seek the location that maximizes the sum of weighted correlations using an L1 norm. The *S* wave velocity model is computed from a 1-D *P* wave velocity V_p model [*Waldhauser et al.*, 2004] by dividing a nominal V_p/V_s ratio of 1.732. This method is very similar to and is a derivative of the methods used in previous studies [*Gomberg et al.*, 2008a; *Peng et al.*, 2008; *Rubinstein et al.*, 2007, 2009a; *Wech and Creager*, 2007; Ghosh et al., submitted manuscript, 2009]. The only difference is that we improve the weighting scheme and include a bootstrapping technique for error analysis. A detailed description of the location technique is given by *Wech and Creager* [2008].

4. Locations of the Triggered Tremor

[18] Figure 1 shows the locations of the 21 tremor sources triggered by 8 teleseismic events, the ambient tremor locations [*Nadeau and Dolenc*, 2005] and background seismicity. The corresponding location information for the 21 triggered tremor sources is listed in Table S2. We were unable to locate the tremor triggered by the 2006 Mw8.3 Kuril Island earthquake because of possible mixture of tremor signals with teleseismic *P* waves of its early aftershocks, and the 2006 Mw8.0 Tonga earthquake because of the relatively weak tremor signals. As was found in previous studies [*Gomberg et al.*, 2008a; *Peng et al.*, 2008; Ghosh et al., submitted manuscript, 2009] and will be discussed below, multiple tremor sources were activated during and immediately after the surface wave of many teleseismic events. Hence, the number of tremor sources is more than 2 times the number of teleseismic events. It is worth noting that we only keep those tremor sources with epicentral error estimates <5 km at 95% confidence level based on bootstrap error estimates. So no doubt we miss some weak tremor and multiple tremor sources that occur too close in time to be located separately.

[19] Out of the 21 epicenters of triggered tremor, 11 (52%) are located south of Parkfield near Cholame, where ambient tremor was first identified [*Nadeau and Dolenc*, 2005]. There is a small cluster of 3 (14%) tremor sources near Bitterwater, California, in the creeping section, and the rest are widely distributed along the creeping section of the SAF. While it is possible that some locations could be poorly constrained, we argue that such a scattered distribution is a genuine feature of the tremor locations for the

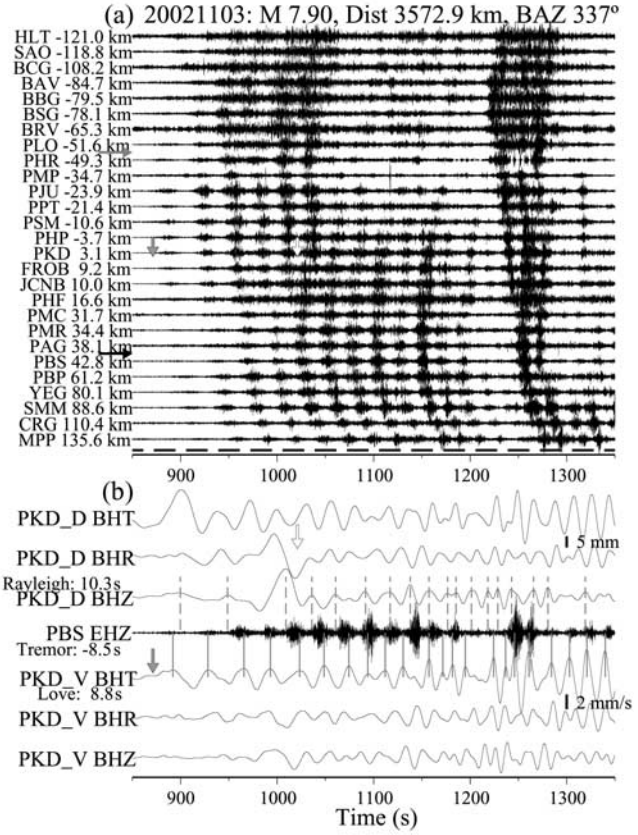

Figure 3. (a) A record section of the 2–8 Hz band-pass-filtered vertical seismograms showing moveout of the tremor from the two source regions (marked by the arrows) triggered by the 2002 Mw7.8 Denali earthquake. The seismograms are plotted according to the along-strike distance on the SAF (shown with the station), with NW on the top and SE on the bottom. The gray and open vertical arrows mark the predicted arrivals of the Love (with the phase velocity of 4.1 km s^{-1}) and Rayleigh waves (with the phase velocity of 3.5 km s^{-1}) at station PKD. (b) A comparison of the time-corrected surface waves recorded at station PKD and band-pass-filtered vertical seismograms at station PBS. Top three traces indicate displacement seismograms recorded at station PKD. The vertical (BHZ) and radial (BHR) components are time shifted by 10.3 s to reflect the travel time of the Rayleigh waves (with the phase velocity of 3.5 km s^{-1}) from the tremor source (marked by the solid arrow) to station PKD. The transverse component (BHT) is time shifted by 8.8 s to reflect the travel time of the Love waves (with the phase velocity of 4.1 km s^{-1}). The middle trace indicates band-pass-filtered vertical seismograms at station PBS, time shifted by −8.5 s to account for the *S* wave travel time between the tremor source and the station. Bottom three traces indicate velocity seismograms recorded at station PKD, with different time shift applied to each component separately. The solid and dashed vertical lines mark the peaks of the Love wave velocity and Rayleigh wave displacement, respectively.

following two reasons. First, the NCSN station distribution is similar in the creeping section north of Parkfield and near Cholame, and the same procedure is applied to locate all triggered tremor within the study region. Hence, the scattered location distribution in the creeping section is unlikely to be caused by the poor station distribution or location technique. Second, ambient tremor locations also show similar patterns [*Nadeau and Dolenc*, 2005; *Nadeau and Guilhem*, 2009]. The majority of the ambient tremor (~95%) is found near Cholame, and the rest is near Monarch Peak in the creeping section of the SAF. The proximity of the ambient and triggered tremor locations suggests that they probably reflect the same tectonic processes. Overall, 20 (95%) the triggered tremor is located within 10 km of the SAF strike (Figure 1a), indicating that tremor is mostly associated with the SAF system.

[20] Although the epicentral location of the triggered tremor source is relatively accurate, the depth is less well constrained, with uncertainties on the order of 10 km. Nevertheless, as shown in Figure 1b, the majority (95%) of the tremor locates in the depth range of 15–31 km, and 9 tremor (43%) locates in the depth range of 24–30 km, near the inferred depth range of the Moho discontinuity around Parkfield [*McBride and Brown*, 1986].

5. Relationship Between Triggered Tremors and Teleseismic Waves

[21] Previous studies have shown that both Love and Rayleigh waves instantaneously trigger tremor [*Gomberg et al.*, 2008a; *Miyazawa and Brodsky*, 2008; *Miyazawa and Mori*, 2005, 2006; *Miyazawa et al.*, 2008; *Peng and Chao*, 2008; *Peng et al.*, 2008; *Rubinstein et al.*, 2007, 2009a; Ghosh et al., submitted manuscript, 2009]. Since Rayleigh waves cause volumetric changes and hence both normal and dilatational stresses at depth, tremor triggered by the Rayleigh waves could be explained by frictional failure or permeability pumping [e.g., *Miyazawa and Brodsky*, 2008]. As was done in previous studies [*Miyazawa and Brodsky*, 2008; *Miyazawa and Mori*, 2006; *Miyazawa et al.*, 2008; *Rubinstein et al.*, 2009a], we interpret upward vertical surface displacement to be indicative of positive dilatational stresses at depth, and examine the relationship between the tremor sources and changes in dilatational stresses caused by the Rayleigh waves.

[22] On the other hand, tremor triggered by the Love waves can only be explained by an instantaneous frictional response to the change of stress state on the plate interface [e.g., *Peng and Chao*, 2008; *Peng et al.*, 2008; *Rubinstein et al.*, 2007, 2009a]. For a near-horizontal plate interface such as seen in a subduction zone, tremor correlates with the Love wave displacement because the displacement amplitude decreases with depth, creating a displacement gradient (i.e., strain) along the near-horizontal interface [*Rubinstein et al.*, 2007, 2009a]. However, for a near vertical plate interface such as the SAF, tremor best correlates with the Love wave ground velocity [*Peng et al.*, 2008; Ghosh et al., submitted manuscript, 2009]. This is because the shear stress resolved on a vertical strike-slip fault aligned with the propagation direction arises from radial direction gradients in the Love wave particle displacement, which is proportional to the velocity [*Hill*, 2008; *Peng et al.*, 2008].

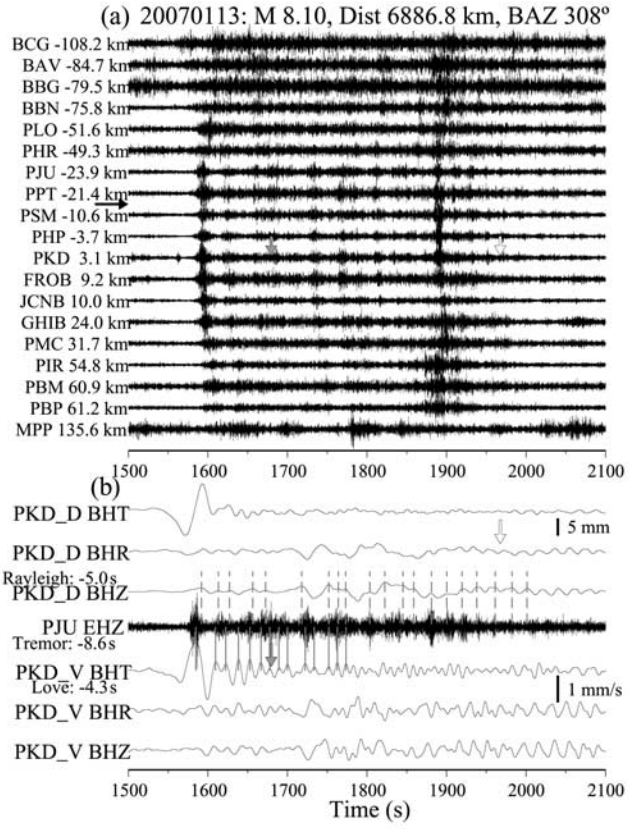

Figure 4. (a) A record section of the 2–8 Hz band-pass-filtered vertical seismograms showing moveout of the tremor from the source region (marked by the arrow) triggered by the 2007 Mw8.1 Kuril Island earthquake. (b) A comparison of the time-corrected surface waves recorded at station PKD and band-pass-filtered vertical seismograms at station PJU. The time shifts for the Rayleigh waves (on the vertical and radial components), the Love waves (on the Transverse component), and the tremor are marked. Other symbols and notations are the same as in Figure 3.

In our case of waves traveling southeast, it is the southwest velocity (i.e., positive peaks) that encourages tremor by boosting right-lateral stress, and the northeast velocity (i.e., negative peaks) that discourages it. Although the focal mechanisms of the SAF tremor and low-frequency earthquakes are not yet known, *Shelly et al.* [2009] found that they form a near-linear structure with strike parallel to the SAF surface waves, indicating that at least portion of the tremor represents shear slip on the deep SAF. Indeed, as found in our previous studies [*Peng et al.*, 2008; Ghosh et al., submitted manuscript, 2009] and will be shown below, the tremor best correlates with the Love wave velocity rather than displacement, further supporting the inference that tremor represents shear slip on the vertical SAF. Because the majority of the teleseismic events occurred along the circum-Pacific seismic belt with the great circle paths close to the SAF strike (Figures 1 and 2), with the exception of two earthquakes from Tonga and Macquarie Islands in southern Pacific Ocean, we rotate the two horizontal components of velocity along and perpendicular to the great circle paths to investigate the relationship between the tremor and stresses induced by Love waves.

[23] Because the tremor signals and surface waves are recorded at different stations, we need to apply a time correction to both signals in order to investigate in detail their causal relationship. For multiple tremor sources that are close to each other, we use the locations corresponding to the longest time window and shift the tremor envelope function with the highest SNR (which is often but not always associated with the nearest station) back to the tremor source region based on the travel time predicted from the 1-D velocity model and the tremor location. For the Love waves, we first compute the difference in the great circle distance (measured from the epicenter of the teleseismic event) between station PKD and the tremor epicenter, then estimate the time shift by dividing a constant phase velocity of 4.1 km s^{-1} [*Peng et al.*, 2008]. For the Rayleigh waves, we use a constant phase velocity of 3.5 km s^{-1} [*Miyazawa and Brodsky*, 2008]. As the phase of the surface wave varies little with depth, we do not make a depth phase correction here.

[24] As we will show below, we find a wide range of relationships between the teleseismic waves and tremor sources. We first describe each event separately, and then summarize their behaviors. We sort the 10 events from greatest to least transverse PGV, which is used as a proxy for dynamic stress associated with the teleseismic surface waves (Figure 2a).

5.1. The 3 November 2002 Mw7.8 Denali Fault Earthquake

[25] The 2002 Mw7.8 Denali Fault earthquake generated the strongest PGV among all the 31 teleseisms during the 7-year study period and triggered the strongest tremor along the SAF in central California (Figure 3). Tremor triggered by this event has been analyzed before [*Gomberg et al.*, 2008a; *Peng et al.*, 2008] and is briefly summarized here. Figure 3a show clear moveout of 2–8 Hz band-pass-filtered signals from at least two tremor sources in central California activated during the surface waves of the Denali Fault earthquake. The first source is around Cholame, where the majority of the triggered and ambient tremors have been found before [*Nadeau and Dolenc*, 2005; *Nadeau and Guilhem*, 2009]. The second source is about 90 km further north in the creeping section between Bitterwater and Monarch Peak. After shifting the tremor envelopes and surface waves to the source regions, we find that tremor is initiated by and is in phase with the Love wave particle velocity, at least for the first 7–8 tremor bursts (Figure 3). For the later tremor bursts, tremor aligns with both the Love and Rayleigh waves equally well.

5.2. The 13 January 2007 Mw8.1 Kuril Island Earthquake

[26] The 2007 Mw8.1 Kuril Island earthquake produced the second highest PGV and also triggered clear tremor around Parkfield (Figure 4). On the basis of the tremor moveout, it appears that only one source region about 16 km north of SAFOD is resolvably active during the large-amplitude surface waves. Additional weak tremor may be activated about 80 km north of SAFOD in the creeping section and in the south near Cholame. We did not attempt

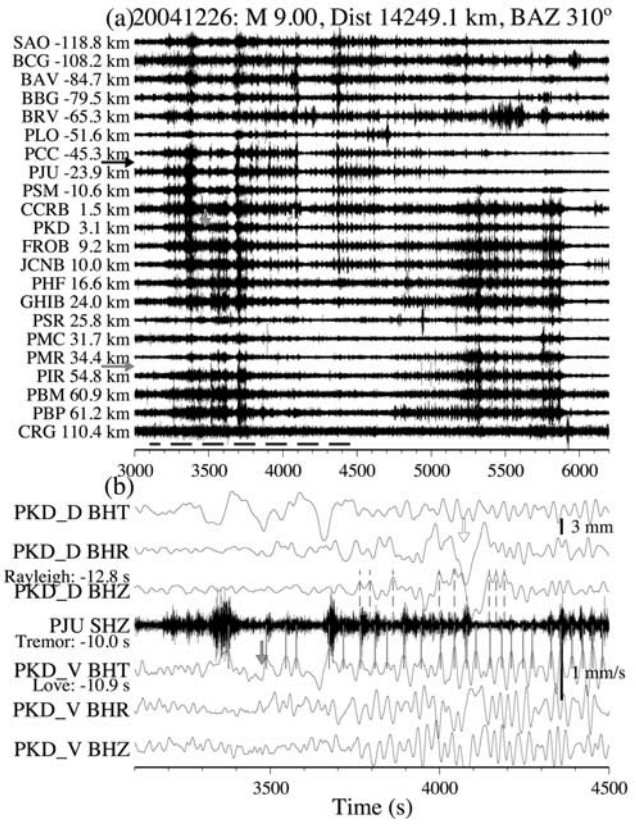

Figure 5. (a) A record section of the 2–8 Hz band-pass-filtered vertical seismograms showing moveout of the tremor from two source regions (marked by the arrows) triggered by the 2004 Mw9.2 Sumatra earthquake. The dashed line corresponds to the time window shown in Figure 5b. (b) A comparison of the time-corrected surface waves recorded at station PKD and band-pass-filtered vertical seismograms at station PJU. Other symbols and notations are the same as in Figure 3.

to locate them due to a relatively small number of observations. After shifting the tremor envelopes and the surface waves back to the inferred tremor source region, we find that the strongest tremor is initiated when the Love wave amplitude is the largest. The tremor continued with similar amplitudes for about 300 s before gradually fading away. While the Love waves are not in phase with the tremor bursts except for the first few bursts, the Rayleigh waves appear to correlate better with the tremor activity, especially between 1900 and 2000 s. This agreement indicates that dilatational stress from the Rayleigh wave may also modulate the tremor occurrence.

5.3. The 26 December 2004 Mw9.2 Sumatra Earthquake

[27] The 2004 Mw9.2 Sumatra earthquake generates the third largest transverse PGV among all the 31 teleseismic events analyzed in this study. Owing to its enormous size and duration, this event was responsible for triggering many small earthquakes in Alaska [*West et al.*, 2005] and tremor in southwest Japan [*Miyazawa and Brodsky*, 2008; *Miyazawa and Mori*, 2006]. Tremor triggered by this earthquake around Parkfield has been extensively studied by Ghosh et al. (submitted manuscript, 2009), and the results are briefly summarized here. Overall, tremor triggered by the Sumatra earthquake lasted for more than 2 h (Figure 5), starting with the passage of the teleseismic *PKP* waves. On the basis of the tremor moveout, at least two source regions were activated, one near Cholame, and the other one between Bitterwater and Monarch Peak, similar to those triggered by the Denali Fault earthquake [*Peng et al.*, 2008]. Both source regions were activated during the Love waves between 3100 and 4100 s. The northern source region continued with another strong episode of activity between 4300 and 5000 s. After that, the northern tremor source gradually turned off. In comparison, the southern source region was not activated between 4000 and 5000 s, became activated again between 5000 and 6000 s, and stopped abruptly near 6000 s. No obvious changes in the surface waves were identified during this period that could correlate with the variations in tremor amplitude in both regions.

[28] In summary, while tremor triggered by the Sumatra earthquake appears to be complicated, it is better correlated with the Love wave velocity rather than the Rayleigh wave displacement (Figure 5). However, the tremor appears to turn on and off on its own, indicating that external stressing

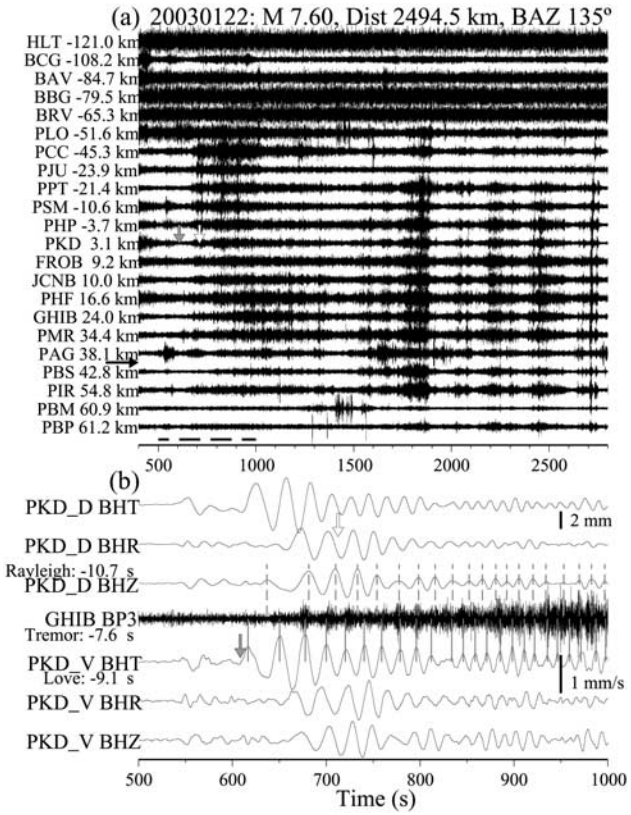

Figure 6. (a) A record section of the 2–8 Hz band-pass-filtered vertical seismograms showing moveout of the tremor from two nearby source regions (marked by the arrows) triggered by the 2003 Mw7.6 Colima earthquake. (b) A comparison of the time-corrected surface waves recorded at station PKD and band-pass-filtered vertical seismograms at station GHIB. Other symbols and notations are the same as in Figure 3.

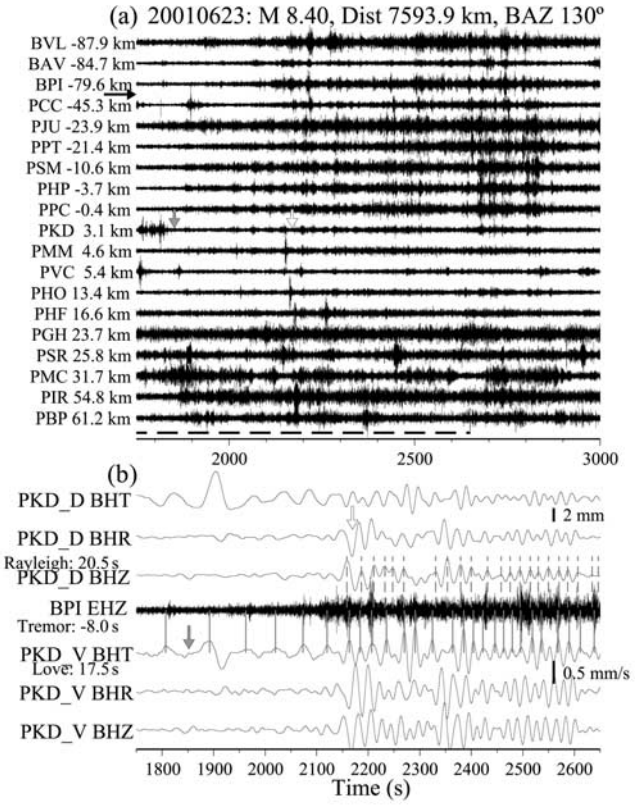

Figure 7. (a) A record section of the 2–8 Hz band-pass-filtered vertical seismograms showing moveout of the tremor from the source region (marked by the arrow) triggered by the 2001 Mw8.4 Peru earthquake. (b) A comparison of the time-corrected surface waves recorded at station PKD and smoothed envelope functions from band-pass-filtered vertical seismograms at station BPI. Other symbols and notations are the same as in Figure 3.

from teleseismic waves help, but is not the only force that controls the behavior of tremor activity.

5.4. The 22 January 2003 Mw7.6 Colima Earthquake

[29] The 22 January 2003 Mw7.6 earthquake in Colima, Mexico also generated strong surface waves and triggered clear tremor south of Parkfield, despite its relatively small magnitude. This is probably because it has an epicentral distance of ~2500 km to station PKD, the closest event we have analyzed in this study. This earthquake triggered multiple episodes of tremor activity during and after the passage of the surface waves (Figure 6). The tremor is mostly active in the south near Cholame. Some weak tremor may have been triggered in the creeping section near Monarch Peak between 600 and 900 s. After correcting for the moveout for both the tremor and surface waves, we find that tremor is in phase with the Love wave velocity for the first 8 cycles. The Rayleigh wave displacements also correlate with some tremor bursts, although the correlation was not as good as the Love waves. The correlation between the tremor and surface wave amplitudes becomes less clear in later periods. The tremor activity between 1500 s and 2800 s is certainly not associated with any clear surface waves, but rather appears to be self-modulated. It's interesting to note that first two cycles of the Love waves have comparable amplitude with latter phases, but they are associated with very weak tremor signals that are barely above the background noise level.

5.5. The 23 June 2001 Mw8.4 Peru Earthquake

[30] The 2001 Mw8.4 Peru earthquake triggered clear tremor that was recorded mainly by the surface stations in the NCSN (Figure 7). The tremor appears to be mostly active in the creeping section of the SAF near Bitterwater. After shifting the tremor and the surface waves back to the source region, we find that some weak tremor with amplitude slightly above the noise level was initiated by and correlated with the Love wave in the first 4–5 cycles before the arrival of the Rayleigh waves. After that, the pattern becomes even less clear. Additional tremor may have been excited at distances of 0–20 km northwest of the SAFOD, because the tremor signals recorded at stations in that section appear to have their own moveout. However, we were unable to obtain reliable location for such a tremor source.

5.6. The 15 November 2006 Mw8.3 Kuril Island Earthquake

[31] The 2006 Mw8.3 Kuril Island earthquake preceded the 2007 Mw8.1 Kuril Island earthquake by 3 months. Despite its larger moment magnitude, the 2006 event has peak transverse PGV that is about 2 times smaller than that for the 2007 event. This could be due to the difference in stress drop or rupture directivity effects [*Ammon et al.*, 2008]. While the tremor signals associated with the 2007 event are clear (Figure 5), it is relatively difficult to analyze the records during the 2006 event. This is because that the 2006 event is followed immediately by a strong aftershock sequence. Some of these aftershocks are large enough to produce high-frequency *P* waves that mix with the tremor signals in the record section (Figure 8). Because of this, we were unable to locate those tremor signals accurately based on 2–8 Hz band-pass-filtered traces. However, we could still identify possible tremor activity north of Bitterwater and in the south near Cholame. On the basis of the apparent timing of the tremor episodes and surface waves arrivals, it appears that some weak tremor occurs near Cholame immediately after the *S* wave arrivals. A relatively strong tremor near Cholame coincides with the Love wave arrivals. After that, more bursts of relatively strong tremor occur in the creeping section around Bitterwater, probably coinciding with the arrival of the Rayleigh waves and continuing afterward for about 1000 s.

5.7. The 12 May 2008 Mw7.9 Wenchuan Earthquake

[32] The disastrous Mw7.9 Wenchuan earthquake in Sichuan, China on 12 May 2008 is the most recent major earthquake that has triggered clear tremor in central California (Figure 9). This event is associated with multiple tremor episodes in at least two regions, one in the creeping section near Bitterwater, and the other one in the south near Cholame. A strong tremor occurred near Cholame immediately after the teleseismic *PKP* phases, similarly to what has been observed for the 2004 Mw9.2 Sumatra earthquake (Ghosh et al., submitted manuscript, 2009). The southern source continued to radiate bursts of tremor between the

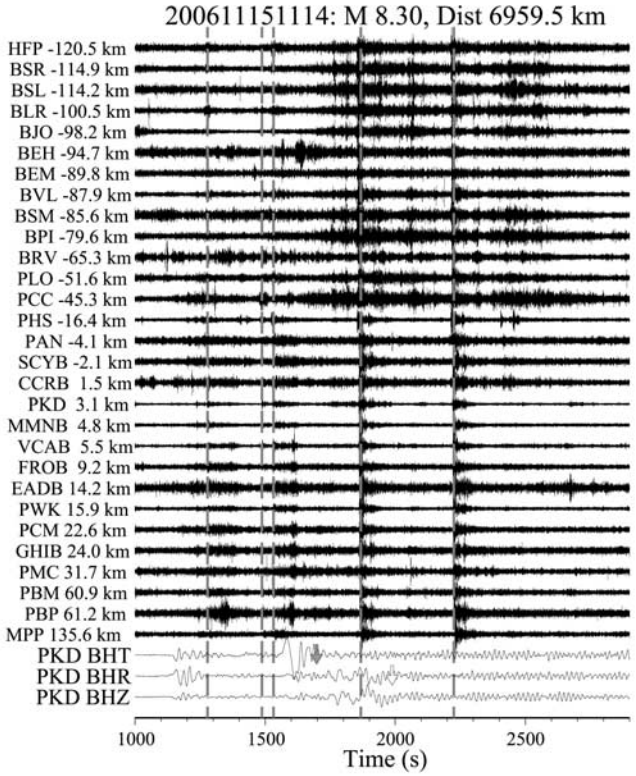

Figure 8. A record section of the 2–8 Hz band-pass-filtered vertical seismograms showing moveout of the tremor triggered by the 2006 Mw8.3 Kuril Island earthquake and the broadband three-component velocity seismograms recorded at station PKD. The vertical dashed lines mark the predicted *P* wave arrival times at station PKD for the five aftershocks with M > 6. The gray and open vertical arrows mark the predicted arrivals of the Love (with the phase velocity of 4.1 km s^{-1}) and Rayleigh waves (with the phase velocity of 3.5 km s^{-1}) at station PKD.

PKP and surface waves, and stepped up activity during the surface waves. Tremor amplitude is better correlated with the Love waves in the first 8 cycles, and then is modulated by both Love and Rayleigh waves at later periods. Another strong tremor occurred at 4000 s, long after the passage of the large-amplitude surface waves.

[33] Compared with multiple episodes of tremor source in the south, the northern tremor source is relatively quiet. It only became active at ~2850 s after a few cycles of the Love waves (Figure S1). The tremor amplitude correlates equally well with both the Love and Rayleigh waves in the first few cycles. A relatively strong burst of tremor occurred at 3500 s, coinciding with a moderate increase of the Love wave amplitude at that time. The pattern is less clear in between when the tremor signals are relatively weak.

5.8. The 25 September 2003 Mw8.3 Tokachi-Oki Earthquake

[34] Triggered tremor was first identified in southwest Japan during the surface waves of the 2003 Mw8.3 Tokachi-Oki earthquake [*Miyazawa and Mori*, 2005; *Miyazawa et al.*, 2008]. This earthquake also triggered clear tremor in Taiwan [*Chao and Peng*, 2008] and around Parkfield (Figure 10). A relatively weak tremor occurs about 17 km NW of the SAFOD between the *S* and Love waves (~1400–1800 s). The distinct tremor burst between 1800 and 1850 s is in phase with a strong peak in the Love waves. More tremor is activated immediately after the arrival of the Rayleigh waves. However, the tremor amplitude does not appear to correlate in phase with either Rayleigh or Love waves. Again, tremor continues on its own long after the passage of the strong surface waves.

5.9. The 14 November 2001 Mw7.8 Kunlun Earthquake

[35] The 2001 Mw7.8 Kunlun earthquake also triggered clear tremor in central California (Figure 11), despite its great distance (>11,400 km), and relatively small PGV (0.017 cm s^{-1} transverse, 0.016 cm s^{-1} vertical). A relatively strong tremor occurred at ~1900 s long before the arrival of the surface waves. This tremor is located in the creeping section of the SAF near Bitterwater (Figure 1). A relatively weak tremor is initiated right at the arrivals of the large-amplitude Love waves. After that, the tremor ampli-

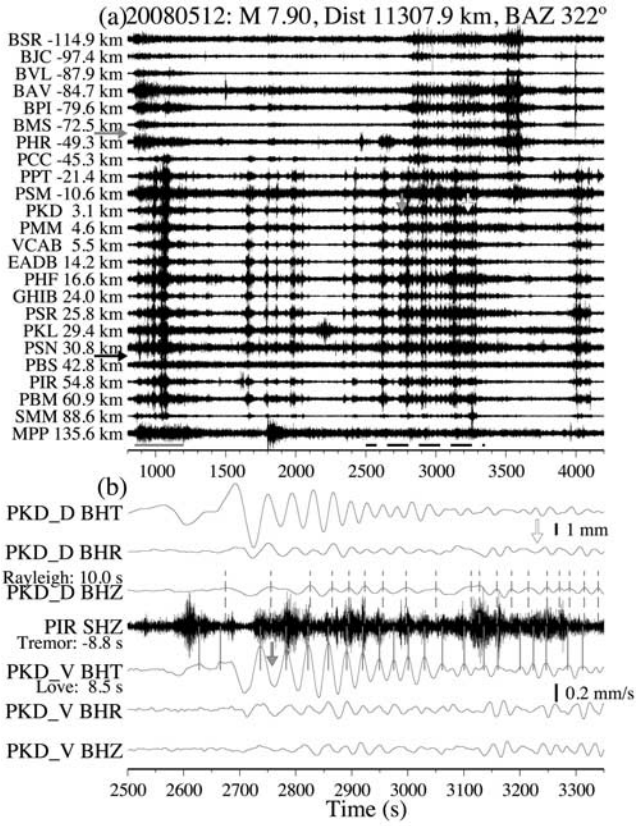

Figure 9. (a) A record section of the 2–8 Hz band-pass-filtered vertical seismograms showing moveout of the tremor from two source regions (marked by the arrows) triggered by the 2008 Mw7.9 Wenchuan earthquake. The horizontal gray lines mark the time window of the PKP phase and the associated tremor. (b) A comparison of the time-corrected surface waves recorded at station PKD and band-pass-filtered vertical seismograms at station PIR. Other symbols and notations are the same as in Figure 3.

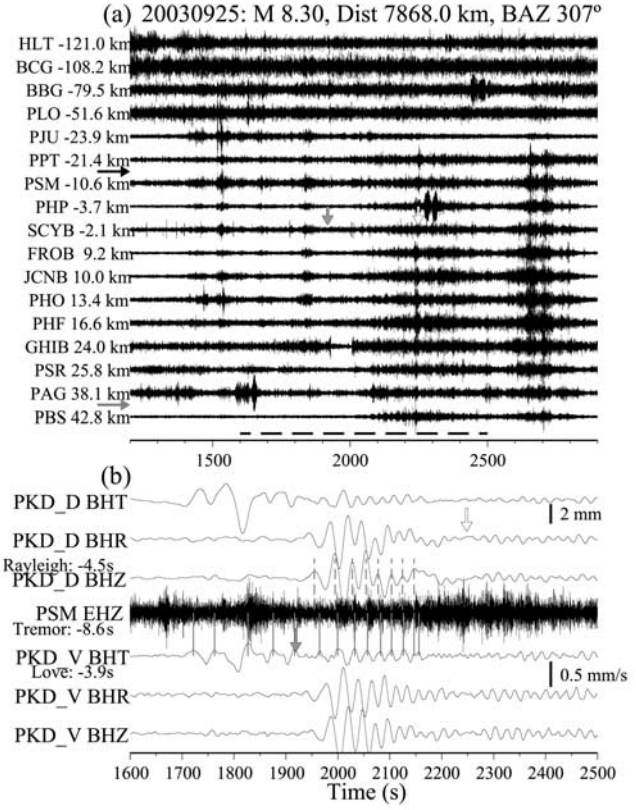

Figure 10. (a) A record section of the 2–8 Hz band-pass-filtered vertical seismograms showing moveout of the tremor from two source regions (marked by the arrows) triggered by the 2003 Mw8.3 Tokachi-Oki earthquake. (b) A comparison of the time-corrected surface waves recorded at station PKD and band-pass-filtered vertical seismograms at station PSM. Other symbols and notations are the same as in Figure 3.

tude is near the noise level, and hence, it is difficult to quantify the relationship with surface wave amplitudes.

5.10. The 3 May 2006 Mw8.0 Tonga Earthquake

[36] The last case was associated with the 3 May 2006 Mw8.0 Tonga earthquake (Figure 12). This earthquake is different as compared with the previous 9 events, because it has raypaths nearly perpendicular to the SAF strike (Figures 1 and 2). Owing to its oceanic path, the long-period surface waves are almost nondispersive and arrive at the same time, as compared the previous cases with clear dispersion for continental paths [*Santo*, 1961]. Nevertheless, some weak tremor occurs between the *S* and Love waves (~1400–1800 s). The tremor is probably located near Parkfield, because it is recorded most clearly by stations in the HRSN. Unfortunately, we were unable to obtain a reliable location based on a relatively small number of observations. Another burst of tremor becomes activated at around 1800 s during the passage of the Love waves. The tremor continues for about 300 s and the amplitude increases at 2000–2100 s during the passage of the large-amplitude Rayleigh waves. Because we did not have an accurate tremor location, we were unable to quantify the exact correlation between the tremor amplitudes and the peaks of the Love and Rayleigh waves.

5.11. Summary

[37] In summary, we have found a rather complicated array of behaviors between the tremor signals and teleseismic waves. In 60% (6 out of 10) of the cases (2002 Denali, 2004 Sumatra, 2007 Kuril Island, 2001 Peru, 2003 Colima, and 2008 Wenchuan), tremor was initiated by the Love waves and was in phase at least for the first few circles. However, the relationship became complicated after the arrival of the Rayleigh waves, and in many cases, tremor continued afterward and turns on and off without any clear relationship with the surface wave amplitudes (e.g., Figures 5 and 10). We also found two cases where tremor occurs during the teleseismic *PKP* phase (2004 Sumatra and 2008 Wenchuan). These observations indicate that while shear stress from the passage of the Love waves plays the most important role in controlling the tremor occurrence and amplitude, other components such as dilatational stress from the Rayleigh and *P* waves also contribute. The self-sustained tremor activity before and after the teleseismic

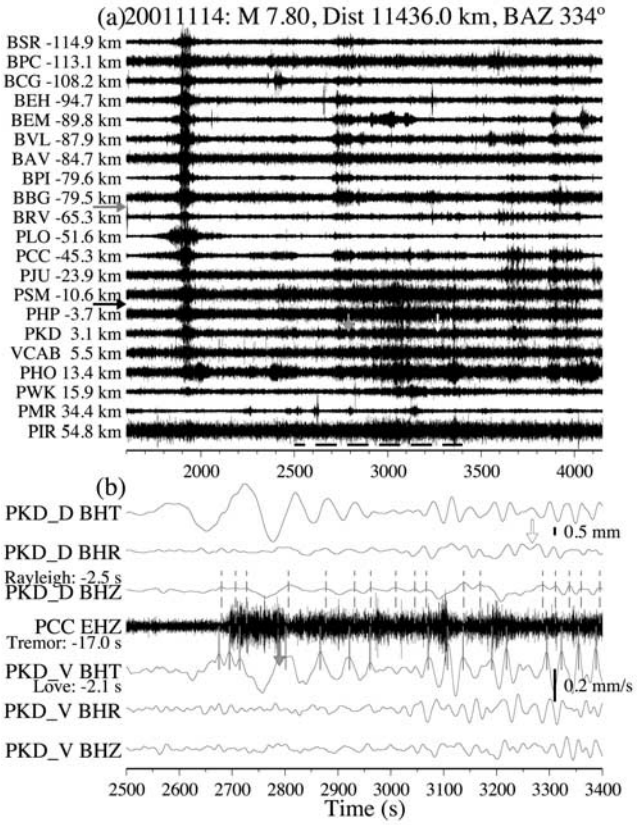

Figure 11. (a) A record section of the 2–8 Hz band-pass-filtered vertical seismograms showing moveout of the tremor from one source region (marked by the arrow) triggered by the 2001 Mw7.8 Kunlun earthquake. (b) A comparison of the time-corrected surface waves recorded at station PKD and band-pass-filtered vertical seismograms at station PCC. Other symbols and notations are the same as in Figure 3.

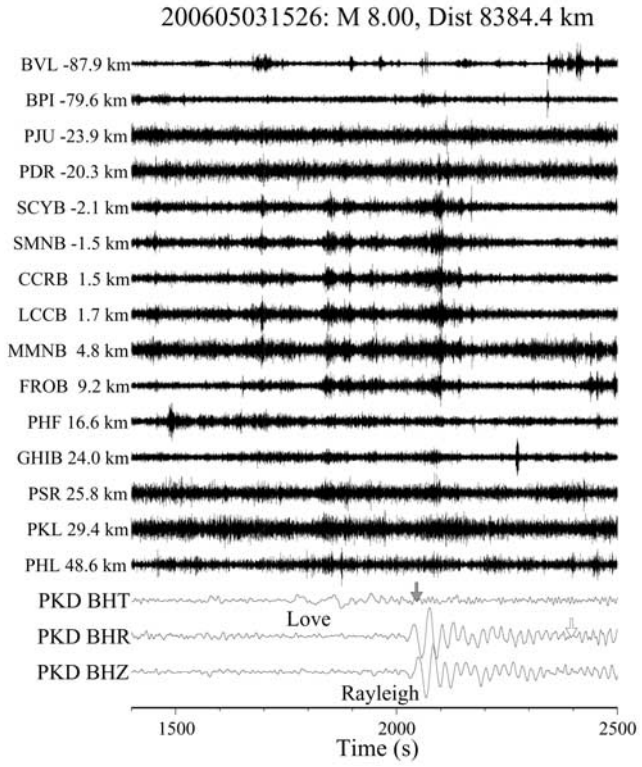

Figure 12. A record section of the 2–8 Hz band-pass-filtered vertical seismograms showing moveout of the tremor triggered by the 2006 Mw8.0 Tonga earthquake, and the broadband three-component velocity seismograms recorded at station PKD. Other symbols are the same as in Figure 8.

surface waves is suggestive of ongoing slow slip or fluid flow [e.g., *Miyazawa and Mori*, 2006].

6. Tremor Triggering Threshold

[38] The wide range of magnitude and distance for the 31 events analyzed in this study allow us to investigate triggering threshold in detail. Previous field observations and laboratory studies have shown that the threshold for dynamic triggering could be a function of both amplitude and frequency [e.g., *Brodsky and Prejean*, 2005; *Gomberg and Davis*, 1996; *Gomberg and Johnson*, 2005; *Hill and Prejean*, 2007; *Savage and Marone*, 2008]. However, the obtained results so far are still inconsistent. For example, *Gomberg and Johnson* [2005] and *Johnson and Jia* [2005] proposed that the maximum amplitude of the seismic waves can be used as a threshold for earthquake triggering, and the mechanisms of dynamic triggering do not strongly depend on frequency. In comparison, *Brodsky and Prejean* [2005] found that low-frequency seismic energy is more effective in triggering seismicity in the Long Valley Caldera than high-frequency energy of the same amplitude.

[39] Recent laboratory studies also found that triggering depends on the amplitude and frequency of the input motion, as well as the stress state of the faults [*Savage and Marone*, 2008]. The later is compatible with the recent results by *Rubinstein et al.* [2009a], who suggested that when a fault is close to failure, or undergoing failure in the case of ongoing tremor and slow slip, it is particularly susceptible for tremor triggering. Because so far no clear slow slip events have been found to accompany tremor activity around Parkfield (e.g., E. F. Smith and J. Gomberg, A search in strainmeter data for slow slip associated with triggered and ambient tremor near Parkfield, California, submitted to *Journal of Geophysical Research*, 2009), here we only quantify the triggering threshold in terms of both amplitude and frequency of the surface waves. We discuss the relationship between triggered and ambient tremor in section 7.

6.1. Triggering Threshold as a Function of Amplitude

[40] Figure 2 shows the transverse and vertical PGVs recorded at the broadband station PKD versus the back azimuth. The four events with the largest transverse PGV (the 2002 Denali Fault, 2007 Kuril Island, 2004 Sumatra, and the 2003 Colima earthquakes) all triggered clear tremor around Parkfield. In addition, the tremor associated with these events was initiated by the Love waves and was in phase with the Love wave velocity at least for the first few cycles. All these events have PGV larger than 0.068 cm s^{-1}.

[41] There are 5 events with transverse PGV between 0.027 and 0.068 cm s^{-1}. All of them except the 2004 Mw8.1 Macquarie earthquake have triggered clear tremor around Parkfield. This event occurred near the Macquarie Ridge plate boundary and preceded the great Mw9.2 Sumatra earthquake only by 3 days. Despite its relatively large transverse PGV, no clear tremor was identified around Parkfield. Below the transverse PGV of 0.027 cm s^{-1}, only two earthquakes, namely, the 2001 Mw7.8 Kunlun earthquake and the 2006 Mw8.0 Tonga earthquake, triggered tremor around Parkfield. The Kunlun earthquake has a similar strike-slip mechanism with the 2002 Denali Fault event, which has triggered clear tremor in Taiwan [*Peng and Chao*, 2008]. As mentioned before, the surface waves of both the Tonga and the Macquarie earthquakes are associated with the oceanic path, and hence the dispersion of the surface waves is quite different compared with the rest of the teleseismic events.

[42] Overall, it appears that there is a weak amplitude threshold that lies around 0.027 cm s^{-1} for the transverse component. PGVs greater than that appear to trigger tremor, with the only exception being the 2004 Mw8.1 Macquarie event. The pattern is similar on the vertical PGVs. All 8 events above 0.035 cm s^{-1} triggered tremor around Parkfield. Below 0.035 cm s^{-1}, only the Kunlun and Wenchuan earthquakes did, and the rest did not.

[43] If we assume plane wave propagation for teleseismic waves, the peak dynamic stress σ_d is proportional to $G\dot{u}/v_s$ [*Jaeger and Cook*, 1979], where G is the shear modulus, $\dot{u}$ is the peak particle velocity, and v_s is the phase velocity. Using a nominal G value of 30 GPa, v_s = 4.1 km s^{-1} for the Love waves, and v_s = 3.5 km s^{-1} for the Rayleigh waves, we estimate the amplitude of the stress levels associated with such a threshold to be 2 kPa for the Love waves and 3 kPa for the Rayleigh waves. We note that the threshold stress identified here is rather weak, and we have a few events that do not satisfy the criteria, suggesting that other parameters may also influence the likelihood of tremor triggering. Nevertheless, the threshold of 2–3 kPa is close to the threshold of 5 kPa for triggered earthquakes in the

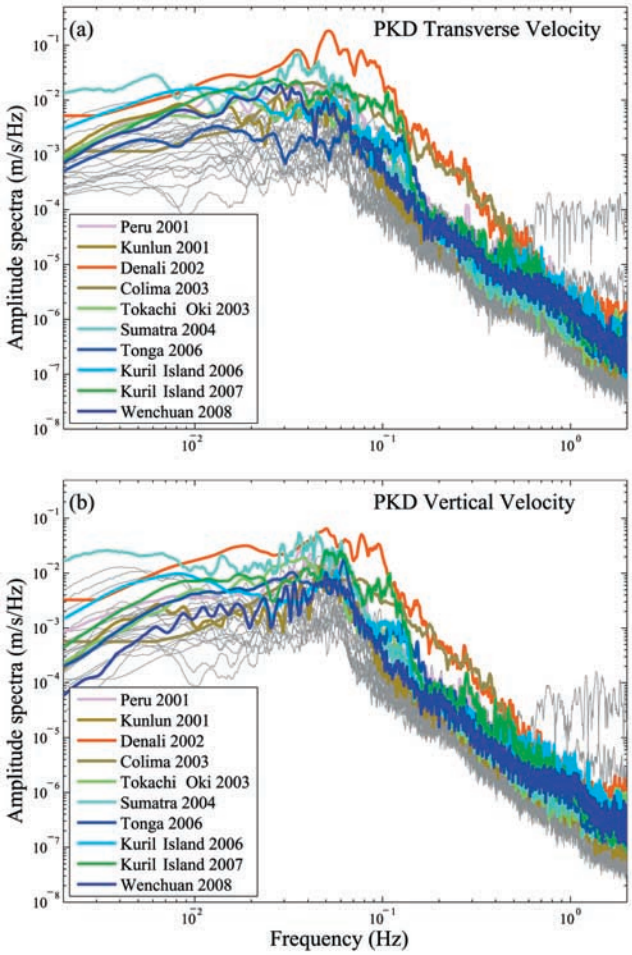

Figure 13. Comparison of the velocity spectra of the (a) transverse and (b) vertical components for the 10 events that have triggered tremor in central California (thick colored lines) with those do not (gray lines).

Long Valley Caldera [*Brodsky and Prejean*, 2005], and recent surveys of triggered tremor in Vancouver Island [*Rubinstein et al.*, 2009a] and Taiwan [*Chao and Peng*, 2008].

6.2. Triggering Threshold as a Function of Frequency

[44] In this section, we attempt to quantify the triggering threshold as a function of input frequency by examining the amplitude spectra recorded at station PKD (Figure 13). We first compute the predicted arrival times that correspond to the velocity of 5 to 2 km s^{-1} to include the majority of the surface wave energy. Then we cut the data within the above time windows, remove the instrument response, and compute the corresponding spectra for both transverse and vertical component seismograms using the fast Fourier transform (FFT) command in SAC [*Goldstein et al.*, 2003]. Finally we smooth the resulting spectra with a sliding window of 10 points. To further help the discussion below, we divide the frequency bands into the following range: longer than 100 s (ultralow-frequency range), between 100 and 10 s (low-frequency range), and between 10 s and 1 s (intermediate frequency range).

[45] Overall, the variations of the spectra are larger for periods longer than 100 s than in the higher frequency range. Such variations are mainly controlled by the rupture dimension of the teleseismic events. For example, the 2004 Mw9.2 Sumatra earthquake has the highest spectra for periods larger than 100 s, because it is associated with a rupture length of at least 1200 km [*Ishii et al.*, 2005], the largest one among all the 31 events analyzed here. However, we find no clear threshold for tremor triggering at periods larger than 100 s on both transverse and vertical components. This suggests that ultralow frequencies (or extremely large earthquakes like the Mw9.2 Sumatra event) are not required to trigger tremor at teleseismic distance.

[46] The surface wave energy is most prominent between 10 to 100 s, especially in the range of 20–60 s. While most of the spectra associated tremor-triggering events are above those for nontremor-triggering events, there is no sharp boundary between these two groups. The transverse component of the 2006 Tonga earthquake falls within the groups of nontremor-triggering events, most likely due to its deficiency in generating Love waves through the oceanic path. For frequencies between 10 and 1 s, the spectra for the two closest events (the 2002 Denali Fault and 2003 Colima earthquakes) are larger than the rest, because the propagation distance also controls the spectra level in this frequency range. While both earthquakes have triggered tremor around Parkfield, other 8 teleseismic events at larger distance also do, and their spectra between 10 and 1 s are marginally above those that do not.

[47] In summary, it appears that seismic energy between 10 to 100 s is likely important in determining whether an earthquake can trigger tremor or not. Again, it is not the only condition that controls the tremor occurrence. Including smaller events at regional distances (100 to 1000 km) would provide a better constraint on whether the relatively high-frequency surface wave energy (e.g., periods smaller than 10 s) has the same ability to trigger tremor as the low-frequency surface wave energy does.

7. Relationship Between Triggered and Ambient Tremor

[48] As briefly described before, triggered and ambient tremor appears to share many common features. These include proximity in epicentral region (at least in Cholame region) and hypocentral depth (typically in the range of 15–30 km), frequency content [*Rubinstein et al.*, 2007; *Peng et al.*, 2008], and polarization characteristics [*Miyazawa and Brodsky*, 2008; *Wech and Creager*, 2007]. Here we further quantify their relationship by comparing our list of triggered tremor with a tremor catalog compiled in central California from 27 July 2001 to 27 May 2008 [*Nadeau and Guilhem*, 2009]. The catalog has a total of 1991 tremor detections, which include both ambient tremor and some triggered tremor analyzed in this study. We first summarize briefly the technique used to compile the ambient tremor catalog. A detailed description of the methodology and properties of this tremor catalog is given by Nadeau and Guilhem (submitted manuscript, 2009). Next, we compare the triggered tremor identified by our visual inspection with those listed in the ambient tremor catalog during the arrivals of large-amplitude surface waves. Finally, we investigate the tremor occurrence rate before, during and after the passage of teleseismic waves.

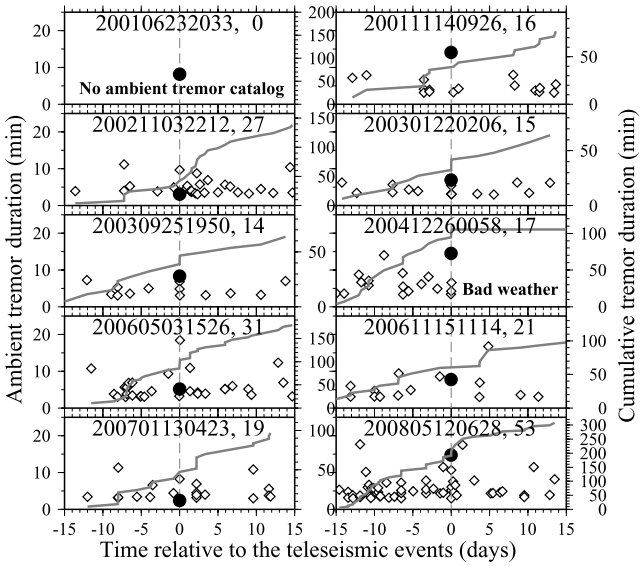

Figure 14. Duration of ambient tremor during the 15 days before and after the 10 teleseismic events that triggered tremor in central California. The duration of the triggered tremor (divided by 3 for plotting purpose) is marked as solid circle. The gray line shows the cumulative tremor duration for each sequence. The teleseismic event ID and number of tremor detections within 30 days are marked on the top of each panel. The ambient tremor catalog started on 27 July 2001, and hence, there is no ambient tremor within 15 days around the 23 June 2001 Mw8.4 Peru earthquake. No ambient tremor is reported for the first few days after the 26 December 2004 Mw9.2 Sumatra earthquake because of a power outage caused by a bad local weather.

7.1. Tremor Catalog

[49] We use the continuous recording of the HRSN to detect 1991 tremor during the study period. On a daily basis, continuous data from a single horizontal component of 8 of the HRSN stations was first filtered with a 3 to 8 Hz passband. Root-mean-square (RMS) envelope seismograms were then generated using a moving 201 sample boxcar window stepped every 0.5 s, yielding RMS seismogram with 2 Hz sampling frequency. Diurnal variations in background noise levels corresponding to cultural activity and cycling of the stations' solar powered systems often exceed 200% of background noise levels in the HRSN data. In addition, there was a change in the HRSN operational parameters in late summer/fall of 2003 to improve the networks sensitivity. Hence for initial detections, determined automatically, we require envelope amplitudes above 300% of background levels since 7 November 2003 for 3 min or longer at 3 or more stations. For days prior to 20 August 2003, amplitudes above 165% of the background levels are selected. Between 20 August 2003 and 6 November 2007, a mix of 300% and 165% were used on a station by station basis as appropriate for the HRSN operational parameter changes.

[50] The filtered and RMS seismograms for the initial detections were then visually inspected to discriminate between tremor signals and amplitude transient artifacts. The visual inspection requires temporal coherence of primary and secondary amplitude fluctuations among at least 3 stations. It also identifies and excludes coherent nontremor activity from earthquake swarms, unusual cultural noise signals (e.g., from deep drilling activity of the SAFOD experiment [*Hickman et al.*, 2004]), and occasional multistation artifacts that can occur during network operations.

[51] Approximately 8% of the initial detections were excluded during the visual inspection process. Also excluded from the analysis are data for the hours of the day following the 22 December 2003, Mw6.5 San Simeon and 28 September 2004, Mw6.0 Parkfield California main shocks and for the entire 2 days following these events. Data for these periods was dominated by amplitude transients from thousands of frequently overlapping early aftershock signals [e.g., *Peng et al.*, 2006], making accurate and complete tremor detections impractical.

[52] A few details warrant additional comment. First, lower amplitude tremor activity also typically occurs nearly every day outside the detection periods, but was not included in the detection catalog. Tests with amplitude thresholds below 300% indicate that between 5 and 10 times the amount tremor activity reflected in the catalog may be detectable (depending on background noise levels), though with significantly lower signal to noise levels and correspondingly greater effort required during visual inspection. In addition, because initial detections require continuously elevated activity for 3 min or longer, some triggered tremor may be missed owing to the multiple shorter durations of amplitude oscillations associated with the passage of the surface waves, particularly during low-amplitude triggered tremor signals.

7.2. Comparison of the Triggered and Ambient Tremor Detection

[53] To identify possible triggered tremor from the ambient tremor catalog, we first compute the expected arrival time of the Love wave at station PKD based on the epicentral distance and the Love wave phase velocity of 4.1 km s^{-1}. Next, we examine the time range from −2000 to 2000 s relative to the Love wave arrivals in the ambient tremor catalog, and find a total of 6 tremor detections around the teleseismic arrivals of the 2002 Denali Fault, 2003 Colima, 2003 Tokachi-Oki, 2004 Sumatra, 2007 Kuril Island, and 2008 Wenchuan earthquakes (Figure 14). All of them are on the list of 10 events that triggered tremor around Parkfield (Table S1). We did not find any tremor detection in the ambient tremor catalog for the 2001 Peru, 2001 Kunlun, 2006 Tonga, and 2006 Kuril Island earthquakes. The Peru earthquake occurred on 23 June 2001 and was outside the time window of the ambient tremor catalog. No tremor was detected during the 2001 Kunlun and 2006 Tonga events probably due to their relatively weak tremor signals, which are visible only on stations near the tremor source (Figures 11 and 12). Those two events also produced relatively weak PGV among the 10 events (Figure 2). No tremor was detected during the surface waves of the 2006 Kuril Island earthquake, most likely due to the contamination of locally triggered signal with teleseismic *P* waves of early aftershocks (Figure 8). In these cases, it is also possible that the requirement of 3 min of continuously elevated amplitude, used for constructing the ambient

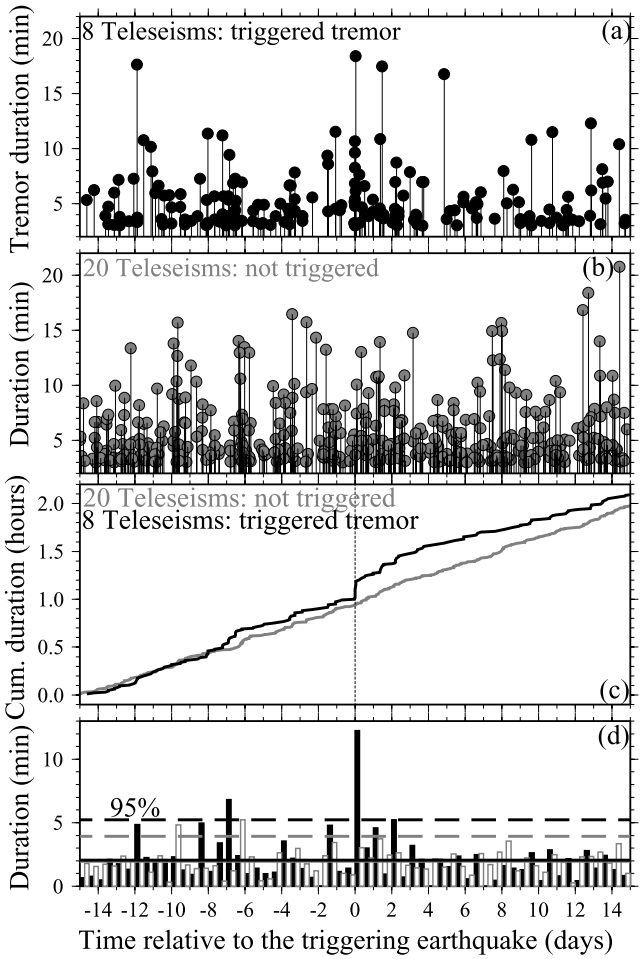

Figure 15. The tremor duration versus the occurrence time of the ambient tremor that occurred between 15 days before and after (a) the 8 earthquakes that triggered tremor in central California and (b) the 20 earthquakes that did not. (c) The cumulative tremor durations (normalized by the number of teleseismic events) for the 8 earthquakes that triggered tremor (black) and the 20 earthquakes that did not (gray). (d) The tremor duration rates per half day that correspond to the 8 earthquakes that triggered tremor (black) and the 20 earthquakes that did not (gray). The black solid and dashed lines mark the mean and the 95% confidence levels measured from data before the triggering event.

tremor catalog, may not have been realized owing to the oscillatory nature of the triggered tremor signal.

[54] Overall, we find a reasonably good match between the triggered and ambient tremor catalog, suggesting that we have visually identified most, if not all the tremor triggered by the 31 events analyzed in this study. The fact that triggered and ambient tremor can be detected by the same technique further supports the inference that they are the same phenomenon but probably just associated with different loading mechanisms.

7.3. Tremor Occurrence Rate Before, During, and After the Teleseismic Events

[55] Finally we examine the ambient tremor activity in the 15 days around the teleseismic surface wave arrivals to identify possible changes caused by the teleseismic events (Figure 14). Out of the 31 teleseismic events analyzed in this study, 29 of them were in the period of the tremor catalog (except the 23 June 2001 Mw8.4 and 7 July 2001 Mw7.6 earthquakes in Peru). We exclude the data associated with the 2004 Mw9.2 Sumatra earthquake because there was power outage for the first few days afterward due to a bad local weather, resulting in an absence of tremor detection in this period. Finally, we divide the remaining 28 events into two groups, 8 events that triggered tremor around Parkfield, and the remaining 20 that did not, and stack the tremor activity in each group for comparison.

[56] Figure 15 shows the stacked tremor activity within 15 days for the 8 and 20 events that did and did not trigger tremor. While the tremor activities associated with the 20 nontriggered events remain stable before and after, there is a noticeable increase of tremor activity at the arrival time of the surface waves for the eight tremor-triggering events. To test the significance of the increase of tremor activity, we sum the tremor duration (normalized by the number of events) in every 12 h for both groups. We then compute the mean and 95% confidence level for the tremor-triggering group for the 15 day time period before the Love wave arrivals. We find that the observed tremor duration within the first 12 h after the Love wave arrivals is clearly above the 95% confidence level, suggesting the observed triggered tremor is not due to random fluctuations of the ambient tremor, but is indeed triggered activity because it is well above the background level. In addition, we find that the tremor activity becomes less frequent after passage of the teleseismic surface waves. Near the end of the 15 day window, the cumulative tremor duration for the eight tremor-triggering events is still above that for the 20 nontremor-triggering event.

8. Discussions and Conclusions

[57] We have conducted a systematic search for remote triggering of tremor along the SAF in central California and found that 10 out of the 31 teleseismic events with Mw $\geq$ 7.5 since 2001 have triggered clear tremor. The triggered tremor concentrates around Cholame south of Parkfield, where most of the ambient tremor has been found before [*Nadeau and Dolenc*, 2005; *Nadeau and Guilhem*, 2009]. The rest is widely distributed in the creeping section of the SAF. Although the depth of tremor is not well resolved at present, our location procedure [*Wech and Creager*, 2008] tends to place tremor near the inferred Moho depth of 25–30 km [*McBride and Brown*, 1986], well below the seismogenic zone of 3–15 km in this region.

[58] Since the location accuracy of our current technique is on the order of 5 km, it is impossible for us to evaluate at this stage whether the triggered tremor was located on the SAF interface, or distributed within a small volume around the SAF. This is mainly because we only use *S* wave travel times to locate the tremor, and that we simultaneously locate multiple tremor bursts that may originate from slightly different regions. Additional sources of systematic bias come from the use of 1-D velocity model in this region [*Waldhauser et al.*, 2004]. Recent studies based on 3-D P wave tomography [*Thurber et al.*, 2006] and fault zone head waves (P. Zhao et al., Variations of the velocity contrast and

rupture properties of M6 earthquakes along the Parkfield section of the San Andreas Fault, submitted to *Geophysical Journal International*, 2009) have shown clear along-strike variations of velocity contrast around the Parkfield section of the SAF. Precise locations of low-frequency earthquakes within tremor near Cholame have found that they form near-linear structures parallel to the SAF strike [*Shelly et al.*, 2009]. Their results suggest that at least some tremor occurs as shear slip on the SAF interface, similar to those found at other major subduction zones [e.g., *Shelly et al.*, 2007a, 2007b; *La Rocca et al.*, 2009].

[59] Our systematic survey of tremor triggered by many teleseismic events allowed us to distinguish among different triggering mechanisms. In 60% of the cases where the teleseismic waves are relatively strong, tremor was initiated by the Love waves and was in phase at least for the first few cycles. However, the casual relationship becomes complicated with the arrival of the Rayleigh waves. In several cases, tremor appears to turns on and off without any clear relationship with the surface wave amplitudes, and sometimes continued after the passage of surface waves (e.g., Figures 5 and 10). The teleseismic *P* waves of the 2004 Sumatra (Ghosh et al., submitted manuscript, 2009) and 2008 Wenchuan earthquakes also triggered clear tremor, despite their relatively small amplitudes (Figures 5 and 8). The overall complicated patterns suggest that while shear stress from the passage of the Love waves plays the most important role in controlling the tremor occurrence and amplitude, other factors, such as dilatational stresses from the Rayleigh and *P* waves also contribute.

[60] *Hill* [2008] performed a theoretical analysis of dynamic triggering of surface waves based on simple Coulomb failure models. Using a Mohr's circle representation, he found that Love waves should have a higher triggering potential than the Rayleigh waves when incident on vertical, strike-slip faults. In addition, he showed that Love waves produce maximum strike-parallel shear stresses on vertical faults for both strike-perpendicular and strike-parallel incidence and purely normal stresses for 45° incidence. His results suggest that the SAF in central California, which is densely instrumented and highly seismogenic, must experience maximum strike-parallel shear stresses from the high-amplitude Love waves when the propagation direction is subparallel to the SAF strike, and should have triggered activity there, in contrary to previous findings [e.g., *Spudich et al.*, 1995; *Prejean et al.*, 2004]. In this study, we found that Love waves are more powerful and better correlate with the tremor than the Rayleigh waves. In addition, most of the tremor triggering events (as well as nontriggering events) generate surface waves with either strike-parallel or strike-perpendicular incidence. Both observations are consistent with *Hill*'s [2008] Mohr's circle analysis and prediction. Recent studies of tide-tremor correlations around Parkfield also found that shear stress fluctuations dominate the triggering process (T. Thomas et al., Tremor-tide correlations and near-lithostatic pore pressure on the deep San Andreas Fault, submitted to *Science*, 2009). However, we also found that Rayleigh and sometimes teleseismic *P* waves also contribute to triggering tremor around Parkfield, suggesting that dilatational stresses are also important in dynamic triggering, as have been proposed before [e.g., *Miyazawa and Mori*, 2006; *Miyazawa and Brodsky*, 2008; *Miyazawa et al.*, 2008].

[61] We hypothesize that the self-sustained tremor activity before and after the teleseismic surface waves marks the presence of ongoing slow slip or fluid flow [e.g., *Miyazawa and Mori*, 2006]. However, contrary to the case of ETS events found in subduction zones, no slow slip events have been found to accompany tremor activity around the Parkfield section of the SAF. Smith and Gomberg (submitted manuscript, 2009) conducted a systematic search of slow slip associated with triggered tremor using continuous data recorded by borehole strainmeters near Parkfield, California, during 11 of the largest of the 31 teleseismic events analyzed in this study. While they did not identify any clear slow slip events during the passage of teleseismic surface waves, they suggested that significant slip could go undetected due the slipping fault's location (particularly depth) and size. Even if strainmeters were directly placed above the slipping fault, a slow slip event with an equivalent moment magnitude of $\sim$5 below the seismogenic zone could go undetected. This leaves open the possibility that smaller slow slip also accompanies tremor in transform boundary settings of California, similar to the ETS phenomenon observed in subduction zones [*Rogers and Dragert*, 2003; *Schwartz and Rokosky*, 2007; *Rubinstein et al.*, 2009b; *Brudzinski and Allen*, 2007; *Brudzinski*, 2008].

[62] The wide range of magnitude and distance for the 31 teleseismic waves permitted us to quantify tremor-triggering threshold in terms of amplitude. We found that the amplitudes of the teleseismic waves play the most important role in controlling the occurrence of triggered tremor. The tremor-triggering threshold around Parkfield is $\sim$2–3 kPa. However, it is worth noting that we also have several outliers (Figure 2), suggesting that other factors also play a role. In terms of the frequency threshold, we found that seismic energy between 10 to 100 s is likely important in determining whether an earthquake can trigger tremor. Periods larger than 100 s or extremely large earthquakes are not required to trigger tremor at teleseismic distance. Since we only focused on teleseismic events, we do not address whether high-frequency waves have the same ability to trigger tremor as low-frequency surface waves do in this study.

[63] We also investigated the relationship between the triggered and ambient tremor around Parkfield. The proximity of the epicentral locations and depth range, and the fact that triggered tremor could also be identified in the regular tremor catalog [*Nadeau and Guilhem*, 2009], suggest that ambient and triggered tremor is probably the same phenomenon but associated with different loading mechanisms. We found that for the stacked sequence, there is a transient increase of ambient tremor activity during large surface wave arrivals and an ensuring decrease of activity afterward (Figure 15). This suggests that the occurrence time of tremor could be temporally advanced by the dynamic stress of the teleseismic waves, resulting in transient increase of tremor activity during large surface waves arrivals. In other words, the small transient loading of teleseismic events leads to ''clock advance'' and triggers tremor that would not have otherwise occurred until the failure threshold was reached by steady far-field plate

motion [e.g., *Gomberg et al.*, 1997, 2000, 2005; *Perfettini et al.*, 2003; *Kaneko and Lapusta*, 2008].

[64] While the transient increase of the stacked tremor rate during and the ensuring decrease after the surface waves are consistent with the "clock advance" model, it is worth noting that the signals are mostly dominated by the 2002 Denali Fault and the 2008 Wenchuan earthquake (Figure 14). This is perhaps not too surprising because the Denali Fault earthquake produced the largest PGV, while the Wenchuan surface waves arrived during one of the elevated tremor episodes [*Nadeau and Guilhem*, 2009]. Since the perturbation failure rate is directly proportional to the background rate times the perturbed stress changes [*Gomberg et al.*, 2000], the "clock advance" effect would be amplified when the background level or the stress perturbations (proportional to PGV) is high. However, we also have several lines of evidence that appear to violate the predication of the clock advance model. First, 4 out of the 10 tremor-triggering events do not have corresponding detection within 2000 s of the Love wave arrivals in the tremor catalog. As mentioned before, the tremor catalog is not available during the 2001 Mw8.4 Peru earthquake. For the 2001 Kunlun and 2006 Tonga event, although there was tremor activity within a few hours afterward, no tremor is found in the catalog during the arrivals of large surface waves. One possible explanation is that either the background level or the stress perturbation is low for these events. Alternatively, the tremor catalog may have missed the weaker or shorter-duration tremor because we did identify triggered tremor associated with these events. In addition, *Gomberg et al.* [2008b] examined both the regular tremor catalog and our triggered tremor events, and found that several large teleseismic events occurred in 2007 (e.g., the 1 April 2007 Mw8.1 Solomon Islands, the 15 August 2007 Mw8.0 Peru, and the 12 September 2007 Mw8.4 southern Sumatra earthquakes) failed to trigger tremor in our study region, although their PGVs and ambient tremor rates are comparable or higher that those from the 2006 Tonga event. Finally, about 48% of the triggered tremor occurred north of Parkfield in the creeping section of the SAF, while only 5% of the ambient tremor occurred in that region. Such a difference could imply that at least some of the triggered tremor is not "clock advanced" ambient tremor. An alternative explanation is the ambient tremor in the creeping section of the SAF is consistently weaker than that near Cholame. Hence, only a small percentage of them with large enough amplitudes are listed in the tremor catalog. In summary, we suggest that the "clock advance" model is supported by our observations only in a statistical sense, and the model so far cannot be applied to predict whether a particular teleseismic event will trigger tremor in central California or not. Further improvement of ambient tremor catalog north of Parkfield and additional tremor triggering events are needed to refine the picture.

[65] It is still not clear why (triggered) tremor concentrates in certain regions of the SAF (e.g., Cholame) and is relatively absent in other places (e.g., directly underneath the Parkfield section of the SAF). While the Cholame section of the SAF was the northern terminus of the rupture and the inferred epicenter of the 1857 Mw7.8 Fort Tejon earthquake [*Sieh*, 1978], it is unclear at this stage whether such correlation is significant or coincidental. *Ellsworth* [2008] found that the two tremor sources triggered by the 2001 Mw7.8 Denali Fault earthquake [*Gomberg et al.*, 2008a; *Peng et al.*, 2008] appear to be spatially correlated with pronounced magnetic highs in central California [e.g., *Griscom and Jachens*, 1990]. Those magnetic anomalies could be associated with a partially serpentinized ultramafic body in the midcrust [e.g., *Hanna et al.*, 1972], which may contain extensive fluids and hence elevated pore pressure. This interpretation is compatible with the weak tremor-triggering threshold of 2–3 kPa, which is several orders of magnitudes smaller than the lithostatic stresses at depth where tremor occurs, suggesting the existence of near-lithostatic fluid pressure [*Hubbert and Rubey*, 1959]. Recent observations of correlation between the tremor onset and tidally induced fault-parallel shear stresses (and lack of correlations with larger normal stresses) also imply low effective normal stresses and near-lithostatic pore pressures in the deep SAF (Thomas et al., submitted manuscript, 2009).

[66] Although the role of metamorphic fluids in the generation of tremor in subduction zones is still debated [e.g., *Kao et al.*, 2005; *Shelly et al.*, 2006, 2007a, 2007b], it is clear that elevated fluid pressure significantly reduces the effective stresses and hence makes tremor more susceptible to external forcing such as tides [*Shelly et al.*, 2007b; *Rubinstein et al.*, 2008; *Nakata et al.*, 2008; Thomas et al., submitted manuscript, 2009] and teleseismic surface waves [e.g., *Gomberg et al.*, 2008a; *Miyazawa and Brodsky*, 2008; *Miyazawa and Mori*, 2005, 2006; *Miyazawa et al.*, 2008; *Rubinstein et al.*, 2007, 2009a; *Peng and Chao*, 2008; Ghosh et al., submitted manuscript, 2009] than regular earthquakes [e.g., *Vidale et al.*, 1998; *Cochran et al.*, 2004]. While many questions remain open, our results indicate that systematic study of triggered tremor helps to quantify the triggering mechanisms and necessary conditions of tremor generation, and improves our understanding of the fundamental processes at the bottom of active faults.

[67] **Acknowledgments.** The data used in this study come from the High Resolution Seismic Network (HRSN) operated by Berkeley Seismological Laboratory, University of California, Berkeley, the Northern California Seismic Network (NCSN) operated by the U.S. Geological Survey, Menlo Park, and are distributed by the Northern California Earthquake Data Center (NCEDC). We thank David Oppenheimer and Doug Neuhauser for extracting the high sampling rate NCSN data used in this study. The manuscript benefited from valuable comments by Joan Gomberg, Justin Rubinstein, two anonymous reviewers, and the Associate Editor. The study was supported by the National Science Foundation (grant EAR-0809834 to Z.P. and grant EAR-0809993 to J.E.V.). Operational support for the HRSN provided through USGS grant 07HQAG0014. Research support for R.M.N. provided through NSF grants EAR-0537641 and EAR-0544730 and through USGS grant 06HQGR0167.

References

Ammon, C. J., H. Kanamori, and T. Lay (2008), A great earthquake doublet and seismic stress transfer cycle in the central Kuril islands, *Nature*, *451*, 561–565, doi:10.1038/nature06521.

Bakun, W. H., and A. G. Lindh (1985), The Parkfield, California, earthquake prediction experiment, *Science*, *229*, 619–624, doi:10.1126/science.229.4714.619.

Bakun, W. H., et al. (2005), Implications for prediction and hazard assessment from the 2004 Parkfield earthquake, *Nature*, *437*, 969–974, doi:10.1038/nature04067.

Brodsky, E. E., and S. G. Prejean (2005), New constraints on mechanisms of remotely triggered seismicity at Long Valley Caldera, *J. Geophys. Res.*, *110*, B04302, doi:10.1029/2004JB003211.

Brudzinski, M. R. (2008), Seismology: Do faults shimmy before they shake?, *Nat. Geosci.*, *1*, 295–296, doi:10.1038/ngeo196.

Brudzinski, M. R., and R. M. Allen (2007), Segmentation in episodic tremor and slip all along Cascadia, *Geology*, *35*(10), 907–910, doi:10.1130/G23740A.1.

Chao, K., and Z. Peng (2008), Remote triggering of non-volcanic tremor around Taiwan, *Eos Trans. AGU*, *89*(53), Fall Meet. Suppl., Abstract U33A-0036.

Chouet, B. A. (1996), Long-period volcano seismicity: Its source and use in eruption forecasting, *Nature*, *380*, 309–316, doi:10.1038/380309a0.

Cochran, E. S., J. E. Vidale, and S. Tanaka (2004), Earth tides can trigger shallow thrust fault earthquakes, *Science*, *306*, 1164–1166, doi:10.1126/science.1103961.

Dragert, H., K. Wang, and T. S. James (2001), A silent slip event on the deeper Cascadia subduction interface, *Science*, *292*, 1525–1528, doi:10.1126/science.1060152.

Ellsworth, W. L. (2008), Origin of nonvolcanic tremor beneath the San Andreas Fault in central California, in *Report on the Aseismic Slip, Tremor, and Earthquakes Workshop*, *U.S. Geological Survey Open File Rep., 2008-1343*, 11.

Goldstein, P., D. Dodge, M. Firpo, and L. Minner (2003), SAC2000: Signal processing and analysis tools for seismologists and engineers, in *The IASPEI International Handbook of Earthquake and Engineering Seismology, Part B*, edited by W. H. K. Lee et al., Chapter 85.5, Academic, London.

Gomberg, J., and S. Davis (1996), Stress-strain changes and triggered seismicity at The Geysers, California, *J. Geophys. Res.*, *101*(B1), 733–749, doi:10.1029/95JB03250.

Gomberg, J., and P. A. Johnson (2005), Seismology-Dynamic triggering of earthquakes, *Nature*, *437*, 830, doi:10.1038/437830a.

Gomberg, J, M. L. Blanpied, and N. M. Beeler (1997), Transient triggering of near and distant earthquakes, *Bull. Seismol. Soc. Am.*, *87*(2), 294–309.

Gomberg, J., N. M. Beeler, and M. L. Blanpied (2000), On rate-and-state and Coulomb failure models, *J. Geophys. Res.*, *105*(B), 7857–7872, doi:10.1029/1999JB900438.

Gomberg, J., P. Reasenberg, M. Cocco, and M. E. Belardinelli (2005), A frictional population model of seismicity rate change, *J. Geophys. Res.*, *110*, B05S03, doi:10.1029/2004JB003404.

Gomberg, J., J. L. Rubinstein, Z. Peng, K. C. Creager, and J. E. Vidale (2008a), Widespread triggering of non-volcanic tremor in California, *Science*, *319*, 173, doi:10.1126/science.1149164.

Gomberg, J, A. Wech, K. C. Creager, D. Christensen, J. Freymueller, P. Bodin, J. E. Vidale, and S. Prejean (2008b), Triggered tremor as a slow slip meter?, *Eos Trans. AGU*, *89*(53), Fall Meet. Suppl., Abstract U32A-01.

Griscom, A., and R. C. Jachens (1990), Crustal and lithospheric structure from gravity and magnetic studies, in *The San Andreas Fault System, California*, edited by R. E. Wallace, *U.S. Geol. Surv. Prof. Pap.*, 1515, 238–259.

Hanna, W. F., R. D. Brown, D. C. Ross, and A. Griscom (1972), Aeromagnetic reconnaissance and generalized geologic map of the San Andreas Fault between San Francisco and San Bernardino, California, *U.S. Geol. Surv. Geophys. Invest. Map, GP-815*.

Hellweg, M., R. A. Uhrhammer, S. Ford, and J. Friday (2008), Nonvolcanic tremor in Denali surface waves at broadband stations in northern California: Instrumental causes?, *Seismol. Res. Lett.*, *79*, 327.

Hickman, S., M. D. Zoback, and W. Ellsworth (2004), Introduction to special section: Preparing for the San Andreas Fault Observatory at Depth, *Geophys. Res. Lett.*, *31*, L12S01, doi:10.1029/2004GL020688.

Hill, D. P. (2008), Dynamic stresses, coulomb failure, and remote triggering, *Bull. Seismol. Soc. Am.*, *98*(1), 66–92, doi:10.1785/0120070049.

Hill, D. P., and S. G. Prejean (2007), Dynamic triggering, in *Treatise on Geophysics*, vol. 4, *Earthquake Seismology*, edited by H. Kanamori, pp. 257–292, Elsevier, Amsterdam.

Hirose, H., and K. Obara (2005), Repeating short- and long-term slow slip events with deep tremor activity around the Bungo Channel region, southwest Japan, *Earth Planets Space*, *57*, 961–972.

Hirose, H., K. Hirahara, F. Kimata, N. Fujii, and S. Miyazaki (1999), A slow thrust slip event following the two 1996 Hyuganada earthquakes beneath the Bungo Channel, southwest Japan, *Geophys. Res. Lett.*, *26*, 3237–3240, doi:10.1029/1999GL010999.

Houston, H., and J. E. Vidale (2007), Earthquakes: Relationships in a slow slip, *Nature*, *447*, 49–50, doi:10.1038/447049a.

Hubbert, M. K., and W. W. Rubey (1959), Mechanics of fluid-filled porous solids and its application to overthrust faulting I, *Geol. Soc. Am. Bull.*, *70*, 115–166, doi:10.1130/0016-7606(1959)70[115:ROFPIM]2.0.CO;2.

Ide, S., G. C. Beroza, D. R. Shelly, and T. Uchide (2007a), A new scaling law for slow earthquakes, *Nature*, *447*, 76–79, doi:10.1038/nature05780.

Ide, S., D. R. Shelly, and G. C. Beroza (2007b), Mechanism of deep low frequency earthquakes: Further evidence that deep non-volcanic tremor is generated by shear slip on the plate interface, *Geophys. Res. Lett.*, *34*, L03308, doi:10.1029/2006GL028890.

Ishii, M., P. M. Shearer, H. Houston, and J. E. Vidale (2005), Extent, duration and speed of the 2004 Sumatra-Andaman earthquake imaged by the Hi-Net array, *Nature*, *435*, 933–936, doi:10.1038/nature03675.

Johnson, P. A., and X. Jia (2005), Nonlinear dynamics, granular media and dynamic earthquake triggering, *Nature*, *437*, 871–874, doi:10.1038/nature04015.

Jaeger, J. C., and N. G. W. Cook (1979), *Fundamentals of Rock Mechanics*, 3rd ed., Chapman and Hall, New York.

Kaneko, Y., and N. Lapusta (2008), Variability of earthquake nucleation in continuum models of rate-and-state faults and implications for aftershock rates, *J. Geophys. Res.*, *113*, B12312, doi:10.1029/2007JB005154.

Kao, H., S.-J. Shan, H. Dragert, G. Rogers, J. F. Cassidy, and K. Ramachandran (2005), A wide depth distribution of seismic tremors along the northern Cascadia margin, *Nature*, *436*, 841–844, doi:10.1038/nature03903.

La Rocca, M., K. C. Creager, D. Galluzzo, S. D. Malone, J. E. Vidale, J. R. Sweet, and A. G. Wech (2009), Cascadia tremor located near plate interface constrained by S minus P wave times, *Science*, *323*, 620–623, doi:10.1126/science.1167112.

Lowry, A. R., K. M. Larson, V. Kostoglodov, and R. Bilham (2001), Transient fault slip in Guerrero, southern Mexico, *Geophys. Res. Lett.*, *28*, 3753–3756, doi:10.1029/2001GL013238.

McBride, J., and L. D. Brown (1986), Reanalysis of the COCORP deep seismic reflection profile across the San Andreas Fault, Parkfield, CA, *Bull. Seismol. Soc. Am.*, *76*, 1668–1686.

Miller, M. M., T. Melbourne, D. J. Johnson, and W. Q. Sumner (2002), Periodic slow earthquakes from the Cascadia subduction zone, *Science*, *295*, 2423, doi:10.1126/science.1071193.

Miyazawa, M, and E. E. Brodsky (2008), Deep low-frequency tremor that correlates with the passing surface waves, *J. Geophys. Res.*, *113*, B01307, doi:10.1029/2006JB004890.

Miyazawa, M., and J. Mori (2005), Detection of triggered deep low-frequency events from the 2003 Tokachi-oki earthquake, *Geophys. Res. Lett.*, *32*, L10307, doi:10.1029/2005GL022539.

Miyazawa, M., and J. Mori (2006), Evidence suggesting fluid flow beneath Japan due to periodic seismic triggering from the 2004 Sumatra-Andaman earthquake, *Geophys. Res. Lett.*, *33*, L05303, doi:10.1029/2005GL025087.

Miyazawa, M., E. E. Brodsky, and J. Mori (2008), Learning from dynamic triggering of low-frequency tremor in subduction zones, *Earth Planets Space*, *60*, e17–e20.

Nadeau, R. M., and D. Dolenc (2005), Nonvolcanic tremors deep beneath the San Andreas Fault, *Science*, *307*, 389, doi:10.1126/science.1107142.

Nadeau, R. M., and A. Guilhem (2009), Nonvolcanic tremor evolution and the San Simeon and Parkfield, California earthquakes, *Science*, doi:10.1126/science.1174155, in press.

Nakata, R, N. Suda, and H. Tsuruoka (2008), Non-volcanic tremor resulting from the combined effect of Earth tides and slow slip events, *Nat. Geosci.*, *1*, 676–678, doi:10.1038/ngeo288.

Obara, K. (2002), Nonvolcanic deep tremor associated with subduction in southwest Japan, *Science*, *296*, 1679–1681, doi:10.1126/science.1070378.

Obara, K., and H. Hirose (2006), Non-volcanic deep low-frequency tremors accompanying slow slips in the southwest Japan subduction zone, *Tectonophysics*, *417*, 33–51, doi:10.1016/j.tecto.2005.04.013.

Obara, K., H. Hirose, F. Yamamizu, and K. Kasahara (2004), Episodic slow slip events accompanied by non-volcanic tremors in southwest Japan subduction zone, *Geophys. Res. Lett.*, *31*, L23602, doi:10.1029/2004GL020848.

Ohmi, S., I. Hirose, and J. J. Mori (2004), Deep low-frequency earthquakes near the downward extension of the seismogenic fault of the 2000 Western Tottori earthquake, *Earth Planets Space*, *56*, 1185–1189.

Payero, J. S., V. Kostoglodov, N. Shapiro, T. Mikumo, A. Iglesias, X. Pérez-Campos, and R. W. Clayton (2008), Nonvolcanic tremor observed in the Mexican subduction zone, *Geophys. Res. Lett.*, *35*, L07305, doi:10.1029/2007GL032877.

Peng, Z., and K. Chao (2008), Non-volcanic tremor beneath the Central Range in Taiwan triggered by the 2001 Mw7.8 Kunlun earthquake, *Geophys. J. Int.*, *175*, 825–829, doi:10.1111/j.1365-246X.2008.03886.x(Fast track).

Peng, Z., J. E. Vidale, and H. Houston (2006), Anomalous early aftershock decay rates of the 2004 M6 Parkfield earthquake, *Geophys. Res. Lett.*, *33*, L17307, doi:10.1029/2006GL026744.

Peng, Z., J. E. Vidale, K. C. Creager, J. L. Rubinstein, J. Gomberg, and P. Bodin (2008), Strong tremor near Parkfield, CA excited by the 2002 Denali Fault earthquake, *Geophys. Res. Lett.*, *35*, L23305, doi:10.1029/2008GL036080.

Perfettini, H., J. Schmittbuhl, and A. Cochard (2003), Shear and normal load perturbations on a two-dimensional continuous fault: 2. Dynamic triggering, *J. Geophys. Res.*, *108*(B9), 2409, doi:10.1029/2002JB001805.

Prejean, S. G., D. P. Hill, E. E. Brodsky, S. E. Hough, M. J. S. Johnston, S. D. Malone, D. H. Oppenheimer, A. M. Pitt, and K. B. Richards-Dinger (2004), Remotely triggered seismicity on the United States west coast following the M_w 7.9 Denali fault earthquake, *Bull. Seismol. Soc. Am.*, *94*, S348–S359, doi:10.1785/0120040610.

Rogers, G, and H. Dragert (2003), Episodic tremor and slip on the Cascadia subduction zone: The chatter of silent slip, *Science*, *300*, 1942–1943, doi:10.1126/science.1084783.

Rubinstein, J. L., J. E. Vidale, J. Gomberg, P. Bodin, K. C. Creager, and S. D. Malone (2007), Non-volcanic tremor driven by large transient shear stresses, *Nature*, *448*, 579–582, doi:10.1038/nature06017.

Rubinstein, J. L., M. La Rocca, J. E. Vidale, K. C. Creager, and A. G. Wech (2008), Tidal modulation of nonvolcanic tremor, *Science*, *319*, 186–189, doi:10.1126/science.1150558.

Rubinstein, J. L., J. Gomberg, J. E. Vidale, A. G. Wech, H. Kao, K. C. Creager, and G. Rogers (2009a), Seismic wave triggering of nonvolcanic tremor, episodic tremor and slip, and earthquakes on Vancouver Island, *J. Geophys. Res.*, *114*, B00A01, doi:10.1029/2008JB005875.

Rubinstein, J., D. R. Shelly, and W. L. Ellsworth (2009b), Non-volcanic tremor: A window into the roots of fault zones, in *New Frontiers in Integrated Solid Earth Sciences*, edited by S. Cloetingh and J. Negendank, Springer, New York, in press.

Santo, T. A. (1961), Dispersion of Love waves along various paths to Japan (Part 1), *Bull. Earthquake Res. Inst. Univ. Tokyo*, *39*, 631–651.

Savage, H. M., and C. Marone (2008), Potential for earthquake triggering from transient deformations, *J. Geophys. Res.*, *113*, B05302, doi:10.1029/2007JB005277.

Schwartz, S. Y., and J. M. Rokosky (2007), Slow slip events and seismic tremor at circum-Pacific subduction zones, *Rev. Geophys.*, *45*, RG3004, doi:10.1029/2006RG000208.

Shelly, D. R., G. C. Beroza, S. Ide, and S. Nakamula (2006), Low-frequency earthquakes in Shikoku, Japan, and their relationship to episodic tremor and slip, *Nature*, *442*, 188–191, doi:10.1038/nature04931.

Shelly, D. R., G. C. Beroza, and S. Ide (2007a), Non-volcanic tremor and low-frequency earthquake swarms, *Nature*, *446*, 305–307, doi:10.1038/nature05666.

Shelly, D. R., G. C. Beroza, and S. Ide (2007b), Complex evolution of transient slip derived from precise tremor locations in western Shikoku, Japan, *Geochem. Geophys. Geosyst.*, *8*, Q10014, doi:10.1029/2007GC001640.

Shelly, D. R., W. L. Ellsworth, T. Ryberg, C. Haberland, G. S. Fuis, J. Murphy, R. M. Nadeau, and R. Bürgmann (2009), Precise location of San Andreas Fault tremors near Cholame, California using seismometer clusters: Slip on the deep extension of the fault?, *Geophys. Res. Lett.*, *36*, L01303, doi:10.1029/2008GL036367.

Sieh, K. (1978), Slip along the San Andreas Fault associated with the great 1857 earthquake, *Bull. Seismol. Soc. Am.*, *68*, 1421–1448.

Spudich, P., L. Steck, M. Hellweg, J. Fletcher, and L. Baker (1995), Transient stresses at Parkfield, California, produced by the M 7.4 Landers earthquake of June 28, 1992: Observations from the UPSAR dense seismograph array, *J. Geophys. Res.*, *100*(B1), 675–690, doi:10.1029/94JB02477.

Thurber, C. H., H. Zhang, F. Waldhauser, J. Hardebeck, A. Michael, and D. Eberhart-Phillips (2006), Three-dimensional compressional wavespeed model, earthquake relocations, and focal mechanisms for the Parkfield, California, region, *Bull. Seismol. Soc. Am.*, *96*(4B), S38–S49, doi:10.1785/0120050825.

Vidale, J. E, D. C. Agnew, M. J. S. Johnston, and D. H. Oppenheimer (1998), Absence of earthquake correlation with Earth tides: An indication of high preseismic fault stress rate, *J. Geophys. Res.*, *103*(B10), 24,567–24,572, doi:10.1029/98JB00594.

Waldhauser, F., W. L. Ellsworth, D. P. Schaff, and A. Cole (2004), Streaks, multiplets, and holes: High-resolution spatio-temporal behavior of Parkfield seismicity, *Geophys. Res. Lett.*, *31*, L18608, doi:10.1029/2004GL020649.

Wech, A. G., and K. C. Creager (2007), Cascadia tremor polarization evidence for plate interface slip, *Geophys. Res. Lett.*, *34*, L22306, doi:10.1029/2007GL031167.

Wech, A. G., and K. C. Creager (2008), Automated detection and location of Cascadia tremor, *Geophys. Res. Lett.*, *35*, L20302, doi:10.1029/2008GL035458.

West, M., J. J. Sanchez, and S. R. McNutt (2005), Periodically triggered seismicity at Mount Wrangell, Alaska, after the Sumatra earthquake, *Science*, *308*, 1144–1146, doi:10.1126/science.1112462.

K. C. Creager, J. E. Vidale, and A. G. Wech, Department of Earth and Space Sciences, University of Washington, 4000 15th Avenue NE, Seattle, WA 98195, USA.

R. M. Nadeau, Berkeley Seismological Laboratory, University of California, Berkeley, 211 McCone Hall, Berkeley, CA 94720, USA.

Z. Peng, School of Earth and Atmospheric Sciences, Georgia Institute of Technology, 311 Ferst Drive, Atlanta, GA 30332, USA. (zpeng@gatech.edu)